ALMA MATER STUDIORUM - UNIVERSITÀ DI BOLOGNA
CAMPUS DI CESENA

DEPARTMENT OF ELECTRICAL
AND INFORMATION ENGINEERING
"GUGLIELMO MARCONI"

SECOND CYCLE DEGREE IN BIOMEDICAL ENGINEERING
CURRICULUM BIOMEDICAL ENGINEERING FOR NEUROSCIENCE

Class: LM-21

ACETYLCHOLINE-MEDIATED NEURAL MASS MODEL FOR EPISODIC MEMORY

Graduation thesis in
NEURAL SYSTEMS

Supervisor
Prof. Mauro Ursino

Candidate
Nicolas Rossi

Co-supervisor
Doct. Gabriele Pirazzini

Academic Year 2023/2024

ACETYLCHOLINE-MEDIATED NEURAL MASS MODEL

FOR EPISODIC MEMORY

"J'y gagne", dit la renard, "à cause de la couleur du blé"
("It has done me good", said the fox, "because of the colour of the wheat fields")

– ANTOINE DE SAINT-EXUPÉRY –

Abstract

Episodic memory is the cognitive skill for the spatiotemporal learning of sequential events. This inborn ability requires the participation of several brain regions, including the entorhinal cortex, the medial septum–ventral diagonal band of the Broca complex, and the hippocampus. Its correct functioning can be explained by means of encoding and retrieval, two separate processes occurring at distinct time intervals: episodic sensorial information is firstly encoded in the hippocampal neurons, then a portion of the previously memorized information, maintained in the working memory, can trigger the retrieval of the entire episode. Unfortunately, the whole mechanism is not completely understood yet, but new studies suggest that acetylcholine (ACh) could play an important role in the regulation of these two phases.
In this thesis a neural mass model, based on the superimposition of theta and gamma rhythms, is proposed to simulate episodic memory based on septal cholinergic release, allowing for the simultaneous encoding and retrieval of temporally coded features. The model exploits different phases of the theta rhythm to avoid interference between the two mechanisms. Hebbian and anti-Hebbian learning methods are employed in the training phase to set the synaptic weights linking the computational areas together. Results, obtained through robustness and sensitivity analyses performed on the parameters defining acetylcholine behaviour, show good resistance to changes, fostering preliminary tests on clinical cases related to damages in cholinergic neural activity. Furthermore, this model was effectively used in simulations of low-ACh physiological states such as quiet waking and slow-wave sleep, demonstrating its reliability for both the theta and non-theta conditions.

Contents

Introduction

In this thesis, a computational neural mass model will be proposed to simulate both the encoding and retrieval phases of episodic memory in the hippocampus, modulated by the effect of acetylcholine.

The first chapter will lay down the basic knowledge of episodic memory to better understand the current state of the art in scientific literature and expose the most important elements that will be resumed later in the model.

In the second chapter, sufficient information about neurocomputational modeling will be provided, touching on all the necessary aspects to acquire an objective and critical point about the main questions and validate the proposed model.

The third chapter will feature an extensive description of the septo/hippocampal model developed, with insights into the technical choices and the commented values of the parameters selected after fine-tuning.

In the fourth chapter, results about the performance of the model will be given, together with robustness and sensitivity analysis.

The last chapter will be an open discussion about what has been achieved and what still needs to be worked on. Some clinical and physiological aspects will be described, such as conditions with overabundance or scarcity of hippocampal acetylcholine, also involving the differences between rapid eye movement sleep and slow wave sleep, related respectively with high and low levels of the neurotransmitter. The chapter will acknowledge both the limitations and future prospects of episodic neurocomputational simulations and present a few directions for further implementations of the model.

With the hope of having aroused your curiosity just as little as to turn the next page, I wish you, with pleasure, a good reading.

Chapter 1

Episodic Memory

1.1 Neural Basis

Episodic memory is the ability to record, retain and recall personal experience as context-based spatiotemporal neurally coded information. In the human brain, and similarly in all mammals and avians [1], the hippocampus and entorhinal cortex are the core elements to elicit such a mechanism.
Neural codes are implied in episodic experience for the simultaneous evaluation of three main aspects: content identification, space localization, and temporal sequencing, or simply the ”what”, ”where” and ”when” codes [2].
The spatial scanning of the environment is executed in the grid cells of the medial entorhinal cortex (MEC) and in the interconnected place cells of the hippocampus, where the receptive field reduces in width from the anterior hippocampus (activated by large-scale locations) to the posterior region (more related to details). MEC grid cells present hexagon-shaped activation patterns, different in phase (orientation of the vertices) and size; besides an apparent random phase organization, the size of grid cells shows a topological distribution, similarly to the hippocampus, with smaller grids in the dorsal border and greater ones in the ventral portion. Thanks to both elements, it takes only a couple of grid cells to entirely cover an environment, initiating and allowing for sparse coding of distinct settings in the hippocampal place cells [2]. The lateral entorhinal cortex (LEC) is also involved in spatial localization but operates more as an earliest contextual integrator for experience, prior to the passage of information to the hippocampus [3]. An initial processing of episodic timing can be found in LEC neurons, too [2].
Perirhinal and Parahippocampal regions account respectively for object extraction and spatial contextualization, acquiring information from the Parietal cortex, which in turn integrates visual and auditory input signals from the Occipital (visual) and Medio-Temporal (auditory) cortices. Both perirhinal and parahippocampal processing results are transmitted to the entorhinal cortex to address the functions formerly reported. Moreover, the Amygdala is implemented as

well in episodic memory, conveying emotional meaning to the otherwise mere spatio-temporal sequences of sensorial stimuli [4].
Up to now, all three "w" codes have been briefly exposed, and at this point a specific region is needed to condense the overall data into coherent, easy-to-read action potentials.
The Hippocampus is, in fact, of utmost importance in the formation of multi-sensory episodic memories, receiving connections and integrating signals from the entorhinal cortex, then projecting to higher cortical levels as well as to up-stream regions through feedback associations. Hippocampal processing starts in the Dentate Gyrus, where sparse coding is implemented for enhancing pattern and features' distinctiveness; it then proceeds into the auto-associative pathway of Cornus Ammonis section 3 (CA3) towards CA1 (first section of CA), finalizing its circuit by sending its messages up to the cortical route, via the necessary mediation of the Subiculum [4].
As it is clear to see, mnemonic abilities in the brain involve several parallel processes to encode multi-sensory and contextualized environmental events into sparse neural firing. The inverse path is also feasible, retrieving information from these almost unique firing patterns back to detailed – or at least, as close as possible – remembrances of the past.
As Miller (1955, [5]), Cowan (2001, [6]), and other researchers have proved over the years of the development of cognitive neuroscience, there is a limit to the amount of distinct elements our brain is able to retain simultaneously in short-term memory, initially uncovered by Miller's 7±2 and eventually reaching Cowan's more likely "magical number" of 4±1. These findings have shown to be valid also for cultural aspects such as linguistics [7] and behavioural economics [8]. But what is behind these numbers, and more importantly, how is it possible for our memories to be precisely encoded into ordered sequences of episodes?

1.2 Theta-Gamma Code

Information delivery in multiple brain regions is regulated through rhythmic oscillations provided by the coordinated collaboration of excitatory (mainly glutamatergic/cholinergic) and inhibitory (GABAergic) neurons. Such waves provide alternate periods of low and high polarization, facilitating and then hindering neural firing while restricting the duration of signal communication to specific segments of time. To obtain such a mechanism, a slow oscillation and a faster one are needed, to respectively organize and then actually convey information. In the hippocampus – the first region found to be displaying this neural code – theta (4 - 10Hz) and gamma ($>$ 30Hz) waves are employed [9] (refer to Figure 1.1 for a representation of theta-gamma cross-frequency coupling).
Theta waves are generated in the Medial Septum/Diagonal Band of Broca complex (MS/DB) and are feed-forwarded towards the hippocampus through

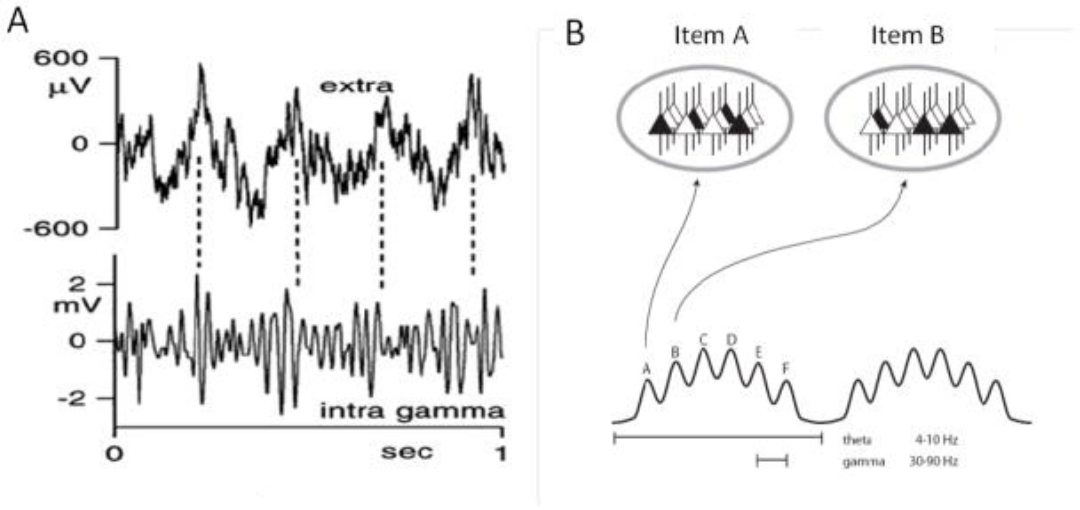

FIGURE 1.1: Theta-gamma neural code. (A) Extracellular (top, theta + gamma) and intracellular (bottom, gamma) recordings of hippocampal activity. (B) Theta-gamma coded schematic representation of ordered items [9].

GABAergic and cholinergic connections [10]. Current evidence additionally suggests the participation of other subcortical structures in theta waves production, mainly supramammillary nucleus and nucleus incertus [11].
Theta-nested gamma waves can be locally generated via feedback connections of fast inhibitory interneurons, which, following the activation of linked pyramidal neurons, promptly polarize the pyramidal population, allowing for high frequency oscillations [12]. Furthermore, gamma waves seem to be modulated as well by the control of MS showing strong phase coupling with hippocampal supra-theta oscillations, although this time following an indirect pathway that from MS projects to the Entorhinal Cortex, passing then from CA3 and ultimately reaching CA1 [11]. More research will be needed to validate this recent finding before its implementation in computational models.
Gamma waves in the hippocampus correlate with sparse neurally encoded feature-based episodes, reflecting subjective sensorial experience. Each episode is evoked by a single gamma cycle, and ordered sequences of episodes are properly clustered inside of the same theta cycle. Based on theta-gamma frequency coupling, a different number of episodes can be correctly maintained in Working Memory (WM), matching Miller's and Cowan's findings.
One typical example of such episodic working memory can be described by the learning of rodents finding their way out of a maze (following the letters of Figure 1.1B): once put on the starting point (A), the maze-runner learns and remembers, both spatially and temporally, the order of each visited turn (e.g. positions A - B - C - D - E - F), building up trial after trial a coherent cognitive map of the presented environment and eventually optimizing its way out of the labyrinth. When placed in a different location, say position C, every other relevant episode will follow afterward, filling all possible theta-nested cycles

with repetitions of the same sequence (C - D - E - F, then again C - D to occupy all 6 of the available gamma-coded items).
Impairments to the MS/DB complex would disrupt theta-gamma coupling, damaging the ordered spatiotemporal episodes and obstructing rodent's working memory capacity, significantly decreasing its ability to complete the maze escape task [10]. Likewise, lesions to MS/DB in humans are related to anterograde amnesia, severely affecting explicit (both semantic and episodic) memory functions, as well as working memory [13].
What has just been described as the neural code of hippocampal information transmission, i.e. the theta-gamma code, is not enough for a functional implementation of working memory. This cross-frequency coupling accounts only for the retrieval of episodes that have been already successfully learned, without explaining their encoding into the neural network. Moreover, it is important for both mechanisms of encoding and retrieval to occur at distinct time frames, since simultaneous learning (of new episodes) and recalling (of old ones) could interfere with neural plasticity, with impairments of Hebbian nature in synaptic and postsynaptic terminals, thus becoming unable to correctly dissociate present and past [14]. A possible solution for this matter could be given by focusing on the population of cholinergic neurons in the medial septum and identifying their specific timing patterns of activation.

1.3 The role of Acetylcholine

Cholinergic projections from the medial septum are one of the main sources of Acetylcholine (ACh) in the central nervous system (CNS), together with the basal nucleus of Meynert and the mesopontine tegmentum area, but become undoubtedly the major one when considering the hippocampus. The neurotransmitter ACh presents multiple effects within the brain, being involved in motivation, arousal, attention and of course, memory: pieces of evidence claim that anticholinergic drugs, such as scopolamine, impairing septo-hippocampal M1 muscarinic receptors, can cause forgetfulness and incapacity in learning new information, while in Alzheimer's disease, a compromised ACh synthesis due to low levels of choline acetyltransferase (ACh catalyst) relates as well with damaged memory [15].
It is common knowledge that ACh presence in the CNS oscillates during the day, showing high levels at waking, especially during arousal, decreasing concomitantly with slow wave sleep (SWS) and reaching high values again during rapid eye movement (REM) sleep, mimicking the waking state (see Figure 1.2). Memory consolidation might operate over the course of low-ACh periods, thus during SWS and idle waking, while the encoding (learning) of sensory-based episodic events is much more likely to occur concomitantly with the high-ACh levels of active waking and REM sleep [16].

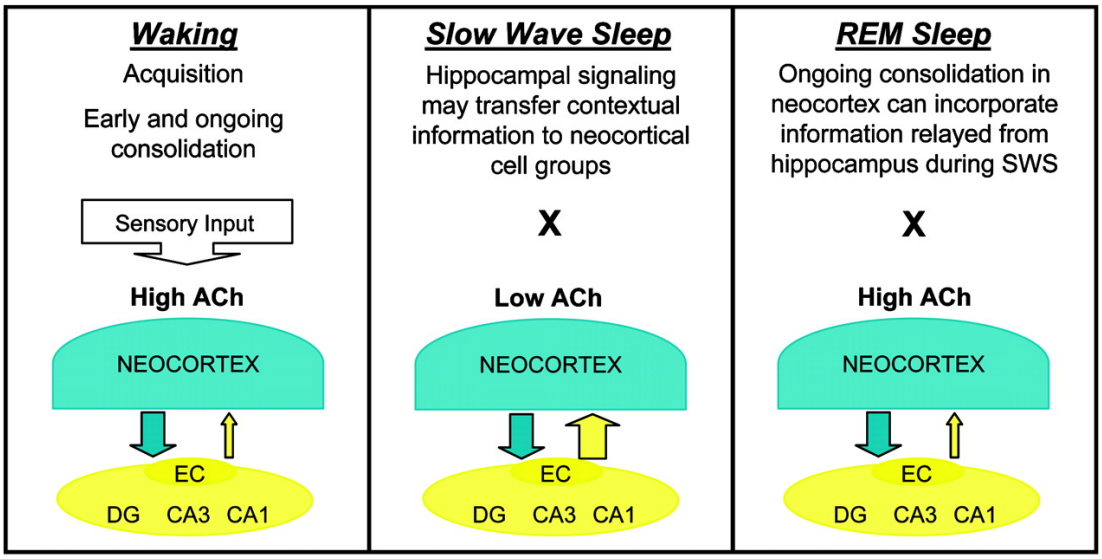

FIGURE 1.2: ACh level-related information flow between neocortex and entorhinal cortex (EC)/hippocampus [16]. (DG: dentate gyrus)

On a similar level, cholinergic oscillations in the hippocampus could discriminate between the encoding (high-ACh state) and retrieval (low-ACh state) of current and previously stored episodes. Cholinergic septal neurons, in fact, fire following theta rhythmicity [17], modulating the connection strength of the different regions of the hippocampus and entorhinal cortex (EC), as shown in Figure 1.3.
During the encoding phase, sensorial information from the EC has priority with respect to CA3 and CA1 regions, which are in turn inhibited to reduce the interference of their stored episodes with the acquisition of new ones, fostering long term potentiation (LTP) of synaptic correlates for input EC episodes. Feedforward connections are thus predominant from EC to both CA3 and CA1. Instead, during the phase of retrieval, feedback connections from CA3 and CA1 prevail, so that already memorized episodes are able to be recovered with minor hindrance from afferent sensorial evidence [17].
This general mechanism allows for both encoding and retrieval to happen in each alternate trough and peak of the theta cycle, meaning that learning and recalling could occur almost simultaneously thanks to the coordination of MS/DB region and its connections to EC and hippocampus. This would also allow the subject to learn a completely new episodic sequence while retrieving a previous one, with positively remarkable consequences in survival.
As previously stated, unbalances in ACh are detrimental to memory. By analysing the system just described, both too high and too low presence of ACh in EC/hippocampus might cause damages in either encoding or/and retrieval: low ACh levels would not enable the strong feedforward connections needed to learn from sensory inputs, impairing the ability to acquire new knowledge and thus compromising encoding; too high ACh levels would certainly potentiate

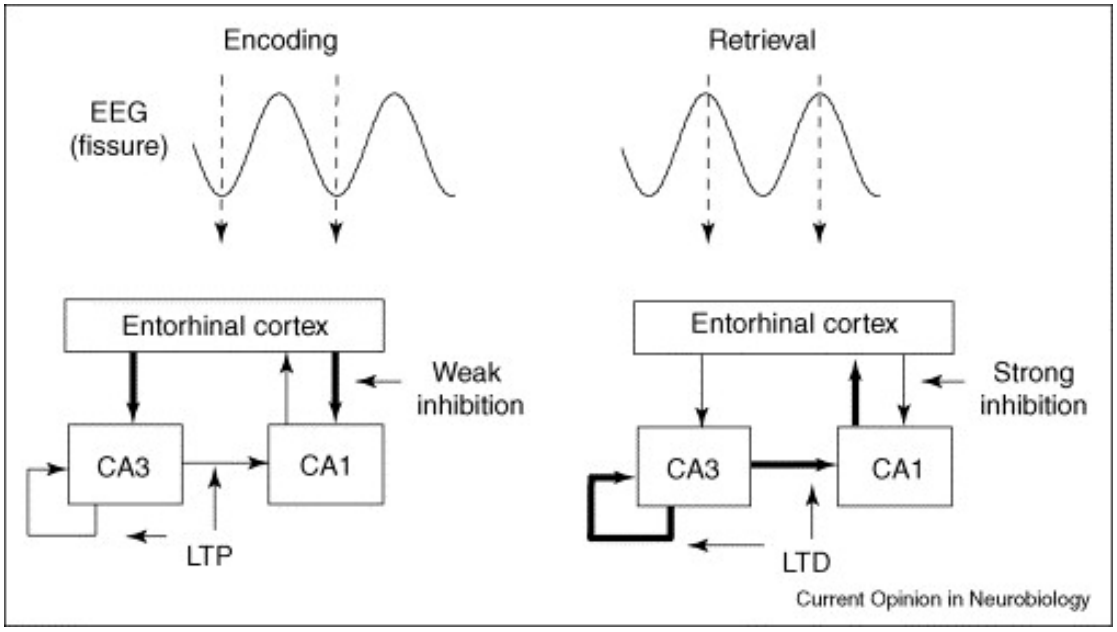

FIGURE 1.3: Cholinergic and theta rhythm anti-synchronicity promoting alternate encoding (enhancing feedforward connections, low theta/high ACh) and retrieval (enhancing feedback, high theta/low ACh) [17].

encoding; however, during retrieval, the feedforward connections from EC to CA3/CA1 would not be inhibited enough to suppress sensory inputs, causing interference of past episodes with new afferent signals, and impairing recall. These conditions will be described in detail in Chapter 3.

1.4 Episodic Encryption

Episodic memory is a powerful skill developed mainly through the complex connections of EC, MS/DB, and hippocampus, allowing us to learn, recall, and then elaborate the information acquired by the sensory evidence of environmental sequential events. Although these subcortical regions exert a major role in this mechanism, it is important to stress the wide interconnections and cooperation that all the main cerebral areas exhibit during episodic encoding and retrieval. All of the inputs perceived by sense organs are sent to the primary sensory regions, but only the most crucial components are evaluated, reducing and optimizing the overall CNS workload. Brain's selectivity in perceptive elements is acquired through plentiful feedback connections implementing constant prediction of the environment, and whatever escapes such anticipatory estimation is tagged with a higher degree of salience, as similarly happens with the targets of attention. By analogy, not all memories are valued the same; some are feeble while others are firmly impressed, shaped by the emotive and volitional state at the time of encoding [18].
The mechanism that underlies this fine-tuning task for the significance-based

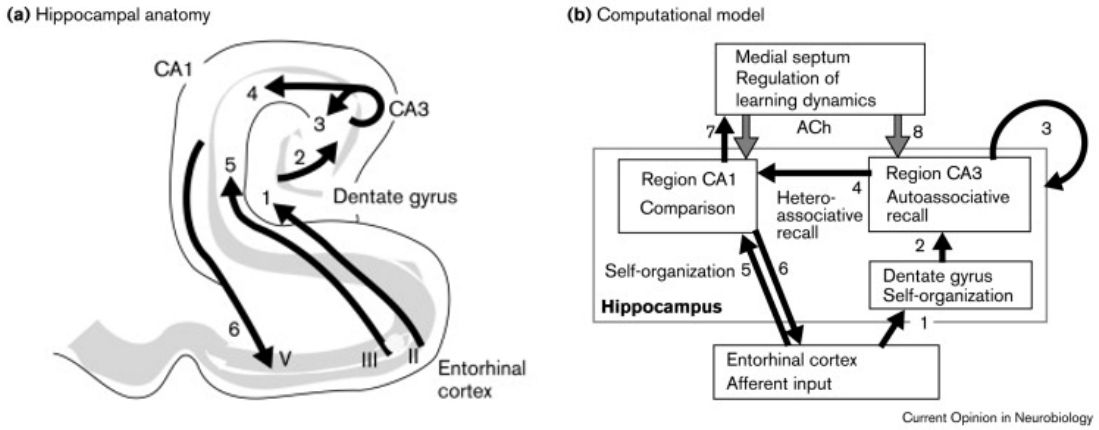

FIGURE 1.4: Hippocampal anatomical pathways (a) and computational model of episodic memory (b) [20].

choice of episodic memory is called emotional valence, controlled by the concurrent activity of Amygdala and Orbito-Frontal Cortex (OFC): the first is implied in understanding the survival importance of certain episodes, modulating visual recognition processing in the presence of fear and rewards, while the second is instead exploited following subject's personal motivation by shifting the attention on what is more interesting to us [18].
The input information, weighted by its emotional valence, is thus processed following a hierarchical structure, passing from low-level features (straightforward characteristics like edges, luminosity and loudness) to high-level ones (more abstract, such as object categories and their spatiotemporal relationship). These properties are essential elements to realize episodic-specific memory traces, or indexes, thanks to the hippocampal pattern separation of the received multisensory features, which majorly take place in the dentate gyrus [19].
Evidence claims that the hippocampus encodes memory indexes along the longitudinal axis based on the extent of the receptive field to be analysed, as previously mentioned, encoding gist-like/general memories in the anterior section, while storing detailed episodic sequences in the posterior region. This resembles neocortical topological functions, with a schematic representation of elements in the anterior portion and a vivid sensory evaluation in the posterior one. Hippocampal indexes are formalized during encoding, but comparable is the process guiding their retrieval: from a small number of relevant features, the hippocampus will select the most significant index – just like in a network of attractors, with extent of each attractor (index) based on its emotional valence – and cooperate with the retrieval of the stored information [19].
Up to now, a synthetic description of the working principles of episodic memory has been discussed in its anatomical, functional and neural aspects, schematized in Figure 1.4. Needless to say, years of research are still needed to achieve a full comprehension of the topic. Neurocomputational modeling remains an interesting tool to provide with critical insights and explain brain functioning in

a numerical setting. How episodic memory could be translated from biological signals to computational simulations will be an intriguing matter of the next pages.

Chapter 2

Neurocomputational Models

2.1 Modeling Neurons

The human brain, composed of 80 - 100 billion electrochemical units, is capable of outstanding parallel computing abilities. Its correct functioning is consistently applied for optimal and coherent decision making in an evolving, often hardly predictable environment. The current level of technology has not yet entirely achieved human reasoning skills, remaining outmatched in either speed, performance, adaptability or energy consumption (with recent progress in neuromorphic computers seemingly approaching human cerebral energetic expenditure [21]).
The first attempts to mathematically emulate the brain's physiological activity focused on the single components, the neuronal cells – particularly on the giant squid axon – analysing the interactions between membrane properties and populations of voltage-dependent ionic channels. Two main experiments were executed, the space clamp (by Marmont and Cole) and the voltage clamp experiment, the latter able to reliably explain the current flowing across the axon as the superimposition of two major ionic currents, produced by sodium and potassium, formally establishing the Hodgkin-Huxley (HH) model [22].
A set of four ordinary differential equations (and even more if considering the effect of other ions) as proposed in the original HH model, although being biophysically accurate, is not the best choice if speed is taken into consideration. FitzHugh introduced a few simplifications to the HH model in order to reduce the number of equations to two, while maintaining the general mechanism intact. With the circuital implementation of Nagumo et al. [23], this mathematical approach became known as the FitzHugh-Nagumo (FHN) model.
By disentangling the physiological aspect from the neuronal action potentials, a new set of computationally applicable formulations can be achieved with obvious advantages (mainly speed) and disadvantages (higher abstraction from real neurons). The simplest model, and overall the first one to be conceived, took the name of integrate-and-fire (IF).

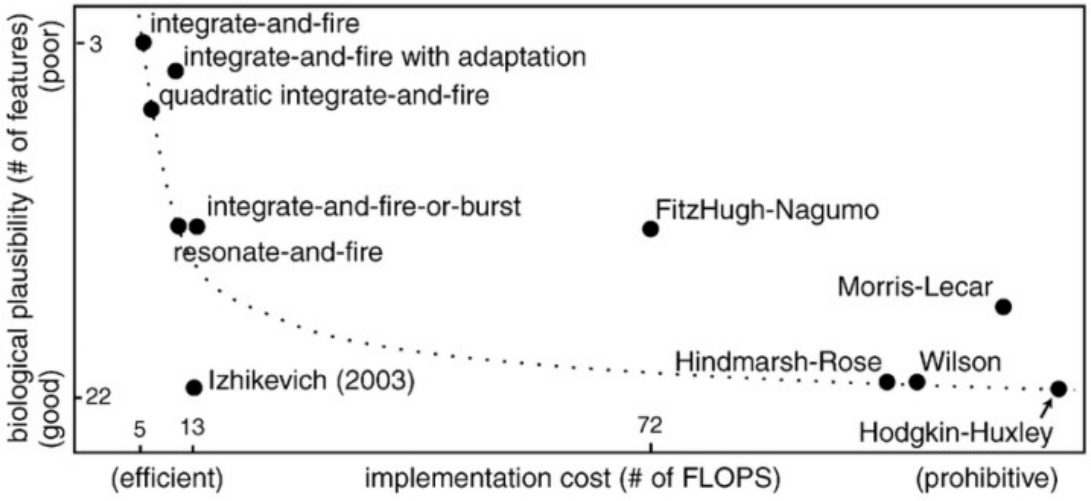

FIGURE 2.1: Comparison of multiple neural computational models in function of implementation cost and biological plausibility [24].

The IF model, in its first stages, was composed of a simple circuit with a resistor and a capacitor in parallel, representing the leakage and capacitance of the membrane. The circuit was charged up to a set threshold and then instantly discharged, producing what is called a "spike", an action potential but degenerated to a single peak of ideally null duration [25].
These spiking neurons, obtained directly from the IF model or from successive variations of the original one, have found utility in the development of spiking neural networks (SNN), achieving smaller energy request and a faster neural implementation with respect to traditional artificial neural networks (ANN).
A comprehensive evaluation of different neural computational models is presented in Figure 2.1, in which the Izhikevich model [26] stands out for blending the biophysiological accuracy of HH and the small cost of IF, allowing for the simulation of a wide range of neuronal types in real-time SNN solutions [27].
One could argue that computational models conceptualized at the level of single neurons should always be preferred over every other possible option, since the emulation of different neural populations and synaptic connections is necessarily the best way to reproduce actual neural networks with the highest accuracy.
Although this is true in ideal conditions, the current energy necessary to compute models of limited brain regions is prohibitive, demanding for the numerical execution of billions of differential equations at every single time step. Furthermore, a stochastic representation of neuronal bursting, coding for spontaneous firing and autonomous chaotic dynamics – obtainable by injecting noise to the system – will add complexity to an already unpractical model.
A certain level of approximation is therefore needed, accomplishable by exploring the mesoscopic size of the human brain and uniforming similar clusters, or masses, of neurons into compact systems.

2.2 Neural Mass Models

2.2.1 Wilson-Cowan Model

To overcome the limitations of neuron-based computational models, and produce a deterministic explanation of events such as pattern recognition, learning and memory, Wilson and Cowan [28] developed a mathematical model combining the effects of populations of excitatory and inhibitory neurons, analysing steady-state and limit cycle occurrences. The two populations were called $E(t)$ and $I(t)$, with respective external inputs $P(t)$ and $Q(t)$.
Multiple hysteresis loops (see Figure 2.2) and limit cycles (Figure 2.3) were achieved by maneuvering excitatory-inhibitory interaction parameters, producing a range of EEG oscillations and validating the link between hysteresis and short-term memory, in which stimuli of enough duration allowed the network to jump from resting to active states. Clearly, these conditions were maintained even after the interruption of the stimulus.

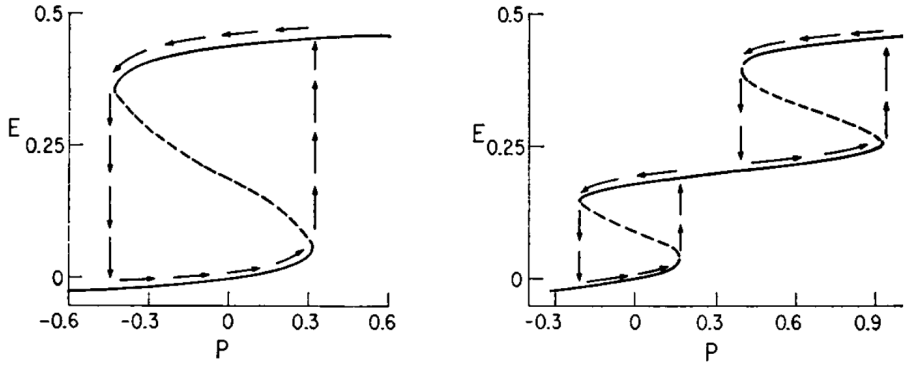

FIGURE 2.2: Phase planes presenting hysteresis, obtained by back-and-forth variation of the input $P(t)$, simple (left) and double (right). Solid lines represent stable states while dashed lines unstable ones [28].

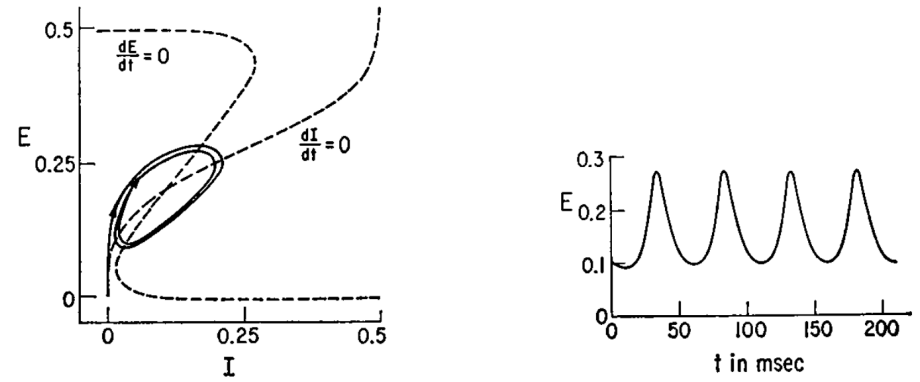

FIGURE 2.3: Phase plane showing a limit cycle (left) and its oscillation in the time domain (right) [28].

A first consideration about the nature of spatial interaction in neural populations can be exploited, as suggested by Wilson and Cowan, by presuming random but dense interconnections between local cells, with the hypothesis that every couple of neurons presents at least one path (straightforward or mediated by interneurons) that binds the pair to the population in study. This way, spatial localization can be neglected, considering a single cellular aggregate.
Second, neural spikes lose their meaning without spatial reference of individual neurons; to explain the activity of the overall population, a distributed spiking frequency was adopted [28].
The third hypothesis of the model was to consider each brain network as result of the interaction between both excitatory and inhibitory neural populations. This assumption was necessary at the time of publication, since a large number of scientific productions in neural modeling was still being developed using exclusively excitatory cells, ignoring a consistent portion of physiological feasibility and incurring in paradoxical conclusions [28].
Successive and present works in neural modeling made extensive use of both populations; however, in most cases, a two-way distinction often resulted in an oversimplification, limiting the model's explainability and functional validation.

2.2.2 Jansen-Rit Model

The simulation of neurophysiologically based cortical columns was proposed by Jansen et al. in 1993 [29] and was then carried on by a joint work with Rit in 1995 [30]. The method used lumped parameters (from Lopes da Silva et al. [31]) to combine the effects of multiple neurons and assimilate their properties into three populations: pyramidal neurons send feedforward information to the other two populations while receiving feedback connections from excitatory and inhibitory interneurons, either basket, stellate or other pyramidal cells.
The input signal was not only received from neighbouring columns, but also from more distal ones, the latter featured in the model as the pulse density $p(t)$ and directly connected with the excitatory interneurons. The pulse density can be any arbitrary function, including white noise, and represents the lumped firing activity (action potentials) of distal cortical columns toward the current one at time t [30].
Each population passes through two blocks, namely an impulse response and a sigmoid normalization. The first transformation converts the pulse density into a lumped postsynaptic membrane potential (called postsynaptic potential or PSP block), while the sigmoid function translates the potential back into firing rate. Since pyramidal neurons and excitatory interneurons share the same synaptic dynamics, both producing excitatory postsynaptic potentials, only two linear transformations were necessary, one for excitatory interneurons and pyramidal neurons, $h_e(t)$, and the other for inhibitory neurons, $h_i(t)$ [30]. The reference blocks of the model are the ones in Figure 2.4.

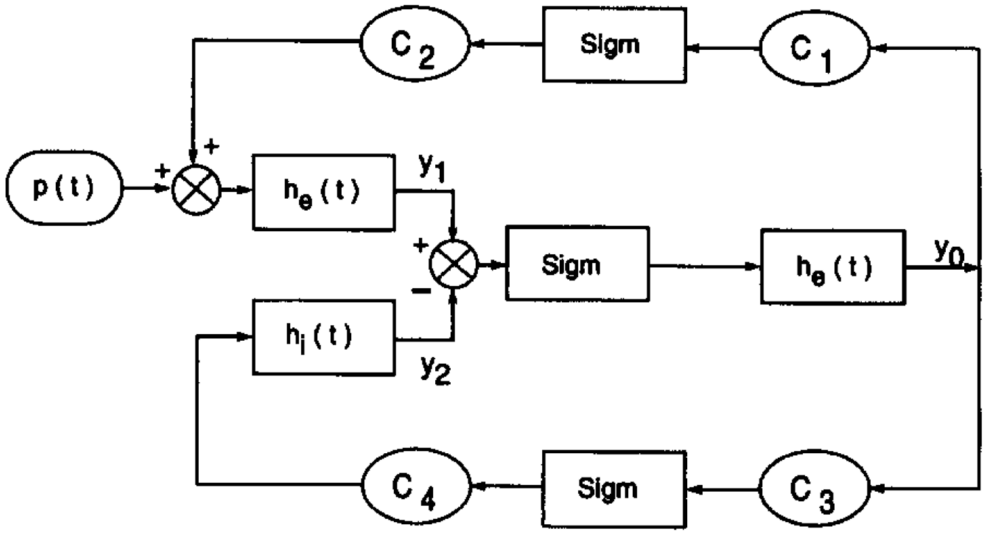

FIGURE 2.4: Jansen-Rit simplified block model for the generation of cortical alpha activity [30].

The impulse responses accounting for the synaptic firing dynamics are defined as:

$$h_e(t) = \begin{cases} Aate^{-at} & t \geq 0 \\ 0 & t < 0 \end{cases} \tag{2.1}$$

$$h_i(t) = \begin{cases} Bbte^{-bt} & t \geq 0 \\ 0 & t < 0 \end{cases} \tag{2.2}$$

being A and B the maximum amplitude of the PSP, excitatory (EPSP) or inhibitory (IPSP), while $a = 1/\tau_e$ and $b = 1/\tau_i$ represent the lumped sum of the inverse of the time constants accounting for all spatially distributed delays, such as in membrane and dendrites.
The sigmoid function is the same for all populations:

$$\text{Sigm}(v) = \frac{2e_0}{1 + e^{r(v - v_0)}} \tag{2.3}$$

with $2e_0$ the maximum firing rate, v_0 the voltage at which the firing rate is half the maximum (e_0), and r being related with the steepness of the sigmoid normalization.
The synaptic connections are represented by four connectivity constants, where C_1 and C_3 are the synaptic ends of the pyramidal neurons toward the excitatory and inhibitory interneurons respectively, and C_2 and C_4 account for connections of the interneurons (excitatory and inhibitory).
The three potentials at the end of the PSP blocks – y_0 for the pyramidal population, y_1 and y_2 for excitatory and inhibitory interneurons – are computed by

means of a second order differential equation:

$$\ddot{y}(t) = Aax(t) - 2a\dot{y}(t) - a^2 y(t) \tag{2.4}$$

The equation just proposed considers the excitatory population. The inhibitory one is likewise described by substituting the constants A/a with B/b. $x(t)$ and $y(t)$ stand for the input (firing rate) and the output (voltage) of the PSP block.
A second order differential equation can always be rewritten as a system of two first order differential equations; this reformulation has the main advantage of improving the computational speed of the model, since it is much easier to solve lower order differential equations by making use of numerical methods from Euler to Runge-Kutta, the latter chosen in the paper.
Given the three populations in study, the final system will be composed of six first order differential equations, and by substituting the subscript 0, 1 and 2 in Figure 2.4 with p (pyramidal), e (excitatory) and i (inhibitory), the system becomes:

$$\begin{cases} \dot{y}_p(t) = z_p(t) \\ \dot{z}_p(t) = Aa\ \mathrm{Sigm}[y_e(t) - y_i(t)] - 2az_p(t) - a^2 y_p(t) \\ \dot{y}_e(t) = z_e(t) \\ \dot{z}_e(t) = Aa\{p(t) + C_2\ \mathrm{Sigm}[C_1 y_p(t)]\} - 2az_e(t) - a^2 y_e(t) \\ \dot{y}_i(t) = z_i(t) \\ \dot{z}_i(t) = Bb\{C_4\ \mathrm{Sigm}[C_3 y_p(t)]\} - 2bz_i(t) - b^2 y_i(t) \end{cases} \tag{2.5}$$

Studies about cortical connectivity in cats and mice were implemented to simplify the constants C_1 to C_3, obtaining that $C_1 = C_2/0.8 = 4C_3 = 4C_4$, thus allowing the model to be varied by simply changing the parameter $C_1 = C$. A range of cortical oscillatory behaviours was thus acquired by modifying either A, B, C or v_0, namely hypoactive noise, slow periodic oscillations, alpha activity, noisy alpha oscillations, and higher frequencies similar to beta activity.
A double-column model was also analysed, obtained by connecting a second column to the first one by a connectivity parameter K and possibly a delay a_d. Each column received two inputs: the external input, which could differ for every column, and the output of the paired column.
This column coupling provided phase-locked outputs, without introducing major differences to the results obtained earlier from the single-column model.

2.2.3 Wendling Model

Despite the high versatility of Jansen's neural mass model, gamma activity was still not achievable with the suggested three populations of pyramidal neurons and excitatory/inhibitory interneurons. A modification – i.e., the introduction

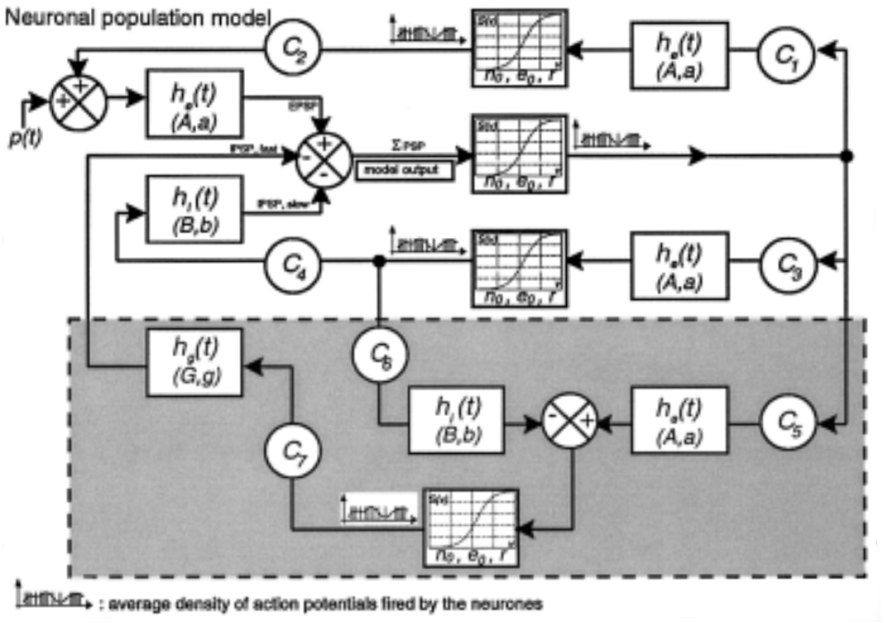

FIGURE 2.5: Wendling block model [32]. The grey rectangle contains the novel blocks, not present in the previously proposed Jansen-Rit scheme.

of a fourth population – was thus needed to push the output oscillatory activity towards higher frequencies, and, in our case, allowing for the simulation of the hippocampal theta-gamma neural code.

For what regards Wendling et al. [32], their studies were oriented towards the simulation of epileptic activity by means of an original neural mass model. Based on relatively new evidence about hippocampal inhibition, two different types of inhibitory postsynaptic currents might have been implied in the formation of the theta-gamma coupling. As a consequence, the choice for a new neural population fell on fast GABAergic interneurons, distinguished from the slow GABAergic activity already exploited in Jansen's work.

The model suggested by Wendling et al. had a construction similar to that just proposed in Figure 2.4, except for the addition of a fourth block for evaluating fast inhibitory interneurons. This population received afferent inputs from both pyramidal neurons and slow GABAergic interneurons, and its output got summed together with the other two populations of interneurons, slow inhibitory and excitatory. An important consequent change introduced in this model regarded the addition of a new PSP block accounting for fast inhibitory synapses, with transformation named h_g, defined as:

$$h_g(t) = \begin{cases} Ggte^{-gt} & t \geq 0 \\ 0 & t < 0 \end{cases} \tag{2.6}$$

which is analogue to Equation 2.1 and 2.2, G being the gain and g the inverse of the time constant, several times bigger than the inhibitory counterpart b (the

chosen values for the time delay parameters were $a = 100s^{-1}$, $b = 50s^{-1}$ and $g = 500s^{-1}$) [32].
Coherently, the differential equations implied from Jansen's system at Equation 2.5 saw the addition of the output $y_g(t)$, from the fast GABAergic population to the pyramidal one, and of $y_{ig}(t)$, from the slow to the fast inhibitory population, with a total of ten first order differential equations:

$$\begin{cases} \dot{y}_p(t) = z_p(t) \\ \dot{z}_p(t) = Aa\ \mathrm{Sigm}[y_e(t) - y_i(t) - y_g(t)] - 2az_p(t) - a^2 y_p(t) \\ \dot{y}_e(t) = z_e(t) \\ \dot{z}_e(t) = Aa\{p(t) + C_2\ \mathrm{Sigm}[C_1 y_p(t)]\} - 2az_e(t) - a^2 y_e(t) \\ \dot{y}_i(t) = z_i(t) \\ \dot{z}_i(t) = Bb\{C_4\ \mathrm{Sigm}[C_3 y_p(t)]\} - 2bz_i(t) - b^2 y_i(t) \\ \dot{y}_g(t) = z_g(t) \\ \dot{z}_g(t) = Gg\{C_7\ \mathrm{Sigm}[C_5 y_p(t) - C_6 y_{ig}(t)]\} - 2gz_g(t) - g^2 y_g(t) \\ \dot{y}_{ig}(t) = z_{ig}(t) \\ \dot{z}_{ig}(t) = Bb\ \mathrm{Sigm}[C_3 y_p(t)] - 2bz_{ig}(t) - b^2 y_{ig}(t) \end{cases} \tag{2.7}$$

as showed in the block diagram of Figure 2.5.
The results obtained by Wendling's model was a realistic simulation of EEG activity in a wide range of frequency bands, including gamma waves, and produced good results in predicting epileptic seizure onsets and transitions between interictal (between seizure) and ictal (during seizure) phases, by altering the three gain parameters A, B and G.
This study demonstrated how neural mass models could be practically involved in the simulation and prediction of cortical and subcortical postsynaptic activity, without the need of an accurate computation at the cellular level, finally paving the way for the exploration of the hippocampal theta-gamma code and its product, episodic memory.

2.2.4 Successive Improvements

Wendling's model was still not perfect: one of the characteristics of EEG measurements is the coexistence of multiple frequency bands in the power spectral density (PSD) of the same region of interest (ROI), in our case theta and gamma rhythms together, but that was not achievable with the four neural groups in question [33]. A new approach would be to consider multiple populations (word that from now on incorporates all the neural types/subpopulations previously stated, i.e. pyramidal neurons and interneurons) interconnected via short- and long-range interactions, so as to generate multiple rhythms by selecting the appropriate parameters.

A neural mass model by Sotero et al. (2007, [34]) realistically reproduced the thalamo-cortical communication via connections between two populations, based on a revised Jansen architecture, simulating the EEG activity at multiple voxels and inferring anatomical connectivity from diffusion weighted magnetic resonance imaging data. In this case, different frequency bands were acquired through variations of the connectivity constant C_1, and through changes in the synaptic time delays, explained by the parameters a, b, and g, singularly producing distributed delta, theta, beta and gamma rhythms, as well as alpha activity. This approach is not ideal for two main reasons: (i) the time constant should be an intrinsic property of synapses, being, in fact, a constant, and should not be manipulated to obtain different wave bands; (ii) no fast inhibitory interneural subpopulation is used in this model, since the two populations shared similarities with Jansen's layout – this could have simplified the generation and control of gamma waves.
One year before Sotero's model, Zavaglia et al. [35] contributed to a study about the simulation of EEG cortical activity based on Wendling's findings. Three populations were implemented with a simplified version of Wendling's model, and the output pyramidal voltage was simply defined as the arithmetic mean of the sum of the outputs from each population.
This time, the connectivity constants were located after each impulse response block, allowing for the merging of the two previously distinct inhibitory PSP blocks, $h_i(t)$, with no more need for the function $y_{ig}(t)$, with a following decrease in the total amount of differential equations from ten to eight. In fact, since the connectivity parameters are constant, and the impulse response is a linear transformation, the error introduced in such modification was practically negligible. The system of differential equations was thus reduced to:

$$\begin{cases} \dot{y}_p(t) = z_p(t) \\ \dot{z}_p(t) = Aa\ \mathrm{Sigm}[C_2 y_e(t) - C_4 y_i(t) - C_7 y_g(t)] - 2a z_p(t) - a^2 y_p(t) \\ \dot{y}_e(t) = z_e(t) \\ \dot{z}_e(t) = Aa\{p(t)/C_2 + \mathrm{Sigm}[C_1 y_p(t)]\} - 2a z_e(t) - a^2 y_e(t) \\ \dot{y}_i(t) = z_i(t) \\ \dot{z}_i(t) = Bb\ \mathrm{Sigm}[C_3 y_p(t)] - 2b z_i(t) - b^2 y_i(t) \\ \dot{y}_g(t) = z_g(t) \\ \dot{z}_g(t) = Gg\ \mathrm{Sigm}[C_5 y_p(t) - C_6 y_g(t)] - 2g z_g(t) - g^2 y_g(t) \end{cases} \tag{2.8}$$

In this model, the parameters describing synaptic kinetics, a, b and g, were kept fixed for each population, while the gains A, B, and G, could instead change, accounting for synaptic plasticity. The three populations were set so that each produced a single type of oscillation, namely in the theta-alpha (4-12Hz), beta

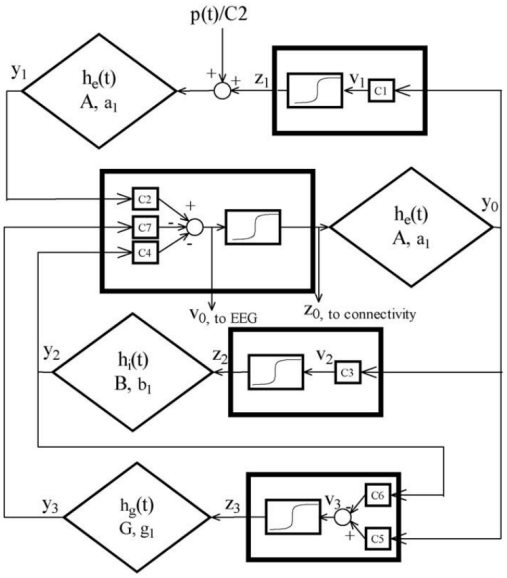

FIGURE 2.6: Zavaglia et al. revised Wendling block model [35].

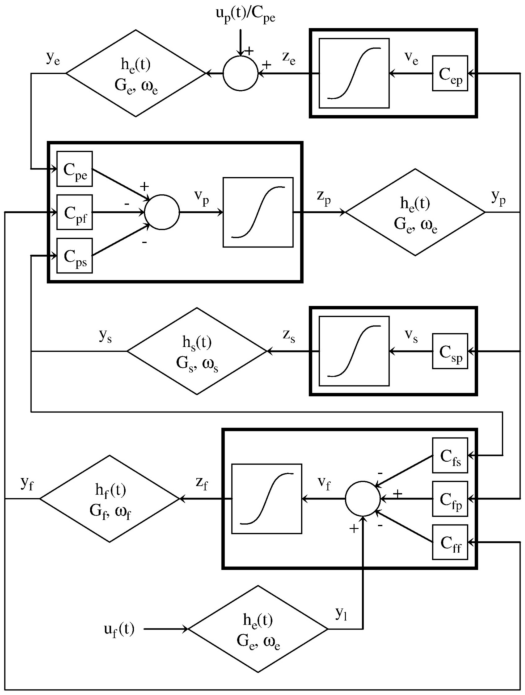

FIGURE 2.7: Ursino et al. [33] block model, variation of Zavaglia et al. [35].

(12-30Hz), and gamma (>30Hz) bands.
The parameter accounting for the fast inhibitory average gain, G, appeared to have greater influence on shifting the PSD peaks. As a result, multiple oscillations were obtained, differently for each ROI under study, mimicking both the power peaks and temporal changes of the gold standard high quality EEG measurements performed.
Obviously, the arithmetic mean of the three populations and their straightforward inputs, consisting merely of noise with fixed mean and standard deviation, described an anatomical and conceptual oversimplification of the connectivity among cortical columns. The last modification of Wendling's model presented here was by Ursino et al. [33], in which a new self-loop was introduced among the fast inhibitory subpopulation, with the addition of a new input for such interneurons, as can be seen from Figure 2.7. These changes had the aim of generating gamma-band oscillations from the exclusive activation of the fast inhibitory portion, independently from the other subpopulations. Such mechanism was included to improve the overall control on the expected PSD shape, which was then perfectible by optimizing the connectivity parameters.
This study made use of a variational model through a revised sigmoid function, now centered at zero, with equation:

$$\mathrm{Sigm}(v) = \frac{2e_0}{1 + \mathrm{e}^{-rv}} - e_0 \tag{2.9}$$

Each parameter thus expressed its variation with respect to a basal value (assumed zero for all). This choice helped maintaining the values in the linear region, avoiding the burden of saturation for specific neural groups due to high levels of connectivity. Consequently, accounting for all the modifications applied, the differential equations could now be written as:

$$\begin{cases} \dot{y}_p(t) = z_p(t) \\ \dot{z}_p(t) = G_e\omega_e \,\mathrm{Sigm}[v_p(t)] - 2\omega_e z_p(t) - \omega_e^2 y_p(t) \\ v_p(t) = C_{pe}y_e(t) - C_{ps}y_s(t) - C_{pf}y_f(t) \\ \dot{y}_e(t) = z_e(t) \\ \dot{z}_e(t) = G_e\omega_e\{u_p(t)/C_{pe} + \mathrm{Sigm}[v_e(t)]\} - 2\omega_e z_e(t) - \omega_e^2 y_e(t) \\ v_e(t) = C_{ep}y_p(t) \\ \dot{y}_s(t) = z_s(t) \\ \dot{z}_s(t) = G_s\omega_s \,\mathrm{Sigm}[v_s(t)] - 2\omega_s z_s(t) - \omega_s^2 y_s(t) \\ v_s(t) = C_{sp}y_p(t) \\ \dot{y}_f(t) = z_f(t) \\ \dot{z}_f(t) = G_f\omega_f \,\mathrm{Sigm}[v_f(t)] - 2\omega_f z_f(t) - \omega_f^2 y_f(t) \\ v_f(t) = C_{fp}y_p(t) - C_{fs}y_s(t) - C_{ff}y_f(t) + y_l(t) \\ \dot{y}_l(t) = z_l(t) \\ \dot{z}_l(t) = G_e\omega_e u_f(t) - 2\omega_e z_l(t) - \omega_e^2 y_l(t) \end{cases} \tag{2.10}$$

with a total of ten first order differential equations, the same number as in Sotero et al. model, solvable with numerical methods in the type of Euler or Runge-Kutta.

This architecture allows good control on the production of gamma band oscillations, which now mainly depend on the fast inhibitory self-loop, and allow for the regulation of multiple bands in PSD evaluations, such as bimodal alpha-gamma spectrum, by simple adjustments to the connectivity parameters.

By connecting several populations of this type and assessing output signal production in specific ROIs, this model has the potential to be implemented in episodic memory simulations, possibly reproducing the hippocampal theta-gamma code for a functional encoding and retrieval of feature-based episodic information.

Needless to say, other interesting neural mass models have been omitted for sake of brevity, for example models by Moran et al. (2007, [36] and 2009, [37]) and Cona et al. (2009, [38]), as well as many previous and successive works.

The notions reported were intended to provide the necessary knowledge about neural mass architectures and denominations, so that the importance of basic elements would not confuse neither hinder the comprehension of more complex

structures, that will be faced in the formal model for episodic memory, right in the next chapter.

Chapter 3

Models for Episodic Memory

Sequential spatiotemporally-organized memories of environmental events are accomplished consistently throughout hours, minutes, and seconds of the brain's active cognitive states, such as active wakefulness and REM sleep.
In the meanwhile, cross-reference analysis of previously experienced episodes with ongoing sensory evidence is assessed in order to predict and validate the possible outcomes, and lead to the best response.
With the aid of neural mass models, it is possible to systematically reconstruct all these functional mechanisms into a deterministic neurocomputational setting, carrying out simulations and tests in a controlled environment. This task is not exactly straightforward, nor trivial, but can be achieved with few variations of the last model seen in Chapter 2.
For a more ordered exposition of the established neurocomputational models, a first system without the regulation of acetylcholine will be treated, accounting for the phase of retrieval and encoding separately; then, the effect of this neurotransmitter will be incorporated, with the purpose of implementing simultaneous encoding and retrieval.

3.1 Theta-Gamma Coupling Model

To start, it is appropriate to review some of the hypotheses and major aspects that are meant to be replicated in computational simulations for episodic memory: (i) Wendling-based neural mass computational models are utilized, which have been proved to be appropriate both for speed and accuracy; (ii) a total of four computational areas is employed, namely working memory (WM), describing the involvement of the medial prefrontal cortex, hippocampal regions CA3 (L1) and CA1 (L2), and the Theta Generator, accounting for septal activity; (iii) the encoding is performed by changing the connectivity between areas, mimicking synaptic plasticity, using Hebbian and anti-Hebbian learning mechanisms for respectively glutamatergic and desynchronizing connections; (iv) each episode is constituted by various features: the majority of them only responds to a single

episode, whereas a small percentage of features is shared among two or more episodes; (v) each temporal sequence is composed of multiple episodes; a correct retrieval is achieved when the totality of the episodic features are consecutively evoked, all in the same theta cycle; (vi) if a single non-shared (orthogonal) feature is given as input, the network should be able to retrieve all other features of the same episode, and later elicit the ordered episodic sequence previously encoded. Each of these aspects will be covered in detail in the next sections. It is worth nothing to say that the model considering ACh influence will present common aspects with the one to be described here; therefore, focus will be given to the significant nuances introduced by the model, disregarding redundant repetitions whenever possible.

3.1.1 The Model

Each computational unit in this work is acquired through a revised Wendling's neural mass model [32] for a single cortical column, formalised by Pirazzini [39] and represented in Figure 3.1. Four neural subpopulations are exploited in the system, namely pyramidal neurons, together with excitatory, slow inhibitory, and fast inhibitory interneurons. Each one is defined by a subscript, in order p, e, s, and f. The pyramidal and fast inhibitory subpopulations admit an input u obtained by summing external signals (E and I), received from other units or from the environment, with random noise n – priorly undergoing a low-pass filtering with glutamatergic dynamics – defining respectively $u_p(t) = E(t) + n_p(t)$ and $u_f(t) = I(t) + n_f(t)$.
Each subpopulation communicates with the others through connectivity constants C. These parameters are reported with two subscripts, the first indicating the target population, while the second specifying its source (for example, C_{ep}

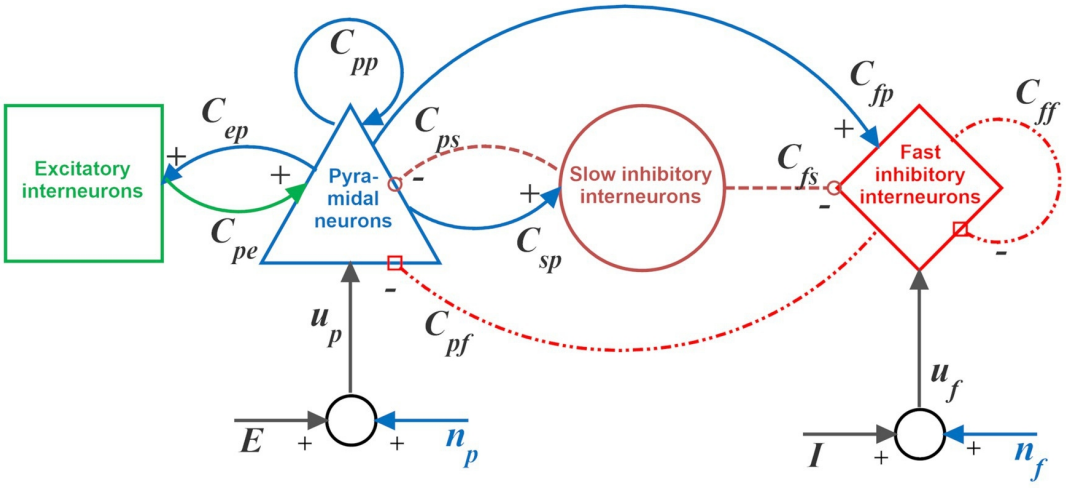

FIGURE 3.1: Schematic representation of a computational unit implementing the theta-gamma coupling, by Pirazzini [39].

means connectivity from pyramidal neurons toward excitatory interneurons). The differential equations involved are the same as the ones exemplified in the last model of Chapter 3 by Ursino et al. [33], reported in Equation 2.10. In this system of ten first order differential equations, the gains are referred with the letter G, while the inverse of the time delays are expressed as pulsations with the letter ω, along with the relative subscript.
Euler method is used for solving the system, with time step of duration 0.1ms. This is, of all, the simplest method to solve differential equations in a computational setting; its major drawback, though, is the necessity of a very small time step to avoid incurring unstable solutions. Other numerical methods, such as Runge-Kutta, could be used to increase the time step and preserve stability and accuracy, improving the computational speed. GPU-based parallel computation could also boost emulation speed [40], especially in the presence of hundreds of possible features and thousands of differential equations altogether, but this will be a matter of future works.
As previously seen, the achieved architecture can generate gamma band oscillations at about 35Hz and slower dynamics. This is essential to permitting responses of hippocampal features within the same theta cycle.
Computational units are wired together by synaptic connections able to change during learning, called weights. These weights bind pre-synaptic pyramidal signals with post-synaptic pyramidal (subscript p) or fast inhibitory (subscript f) subpopulations, thus expressed as either W_p^{YX} or W_f^{YX}; here, the capital W refers to the weights array, composed of all the i-th and j-th interconnections between computational units, reported in lowercase as $w_{p,ij}^{YX}$ or $w_{f,ij}^{YX}$. The superscripts indicate first the target, and then the source of the signal, similarly to the connectivity constants, but this time linking the computational areas (WM, L1, L2, and Theta). For example, W_p^{L1WM} modulates the signal from the working memory toward the hippocampal region CA3, called layer one in the model, reaching the pyramidal subpopulation of each of its units. Furthermore, desynchronizing synapses are utilized to suppress unwanted features at L1, named A_f^{L1L1}.
In Figure 3.2, all computational areas and weights are represented together with a few visual aids, in order to enhance the comprehension of the functioning mechanisms: starting from the perception of a brief and partial episode – in this case, two legs on a floating snowboard – belonging to an already encoded temporal sequence of events, a single distinguishing feature – for example the snowboard colour pattern – is extracted and forwarded to the working memory. Thanks to WM pyramidal self-loop, the active feature undergoes a positive feedback, remaining available in its saturation state even after the perceptual evidence has ceased to occur. Subsequently, the first hippocampal layer L1 receives information from WM and from the Theta Generator (medial septum), integrating them, and retrieving, on each theta peak, the correct sequence of

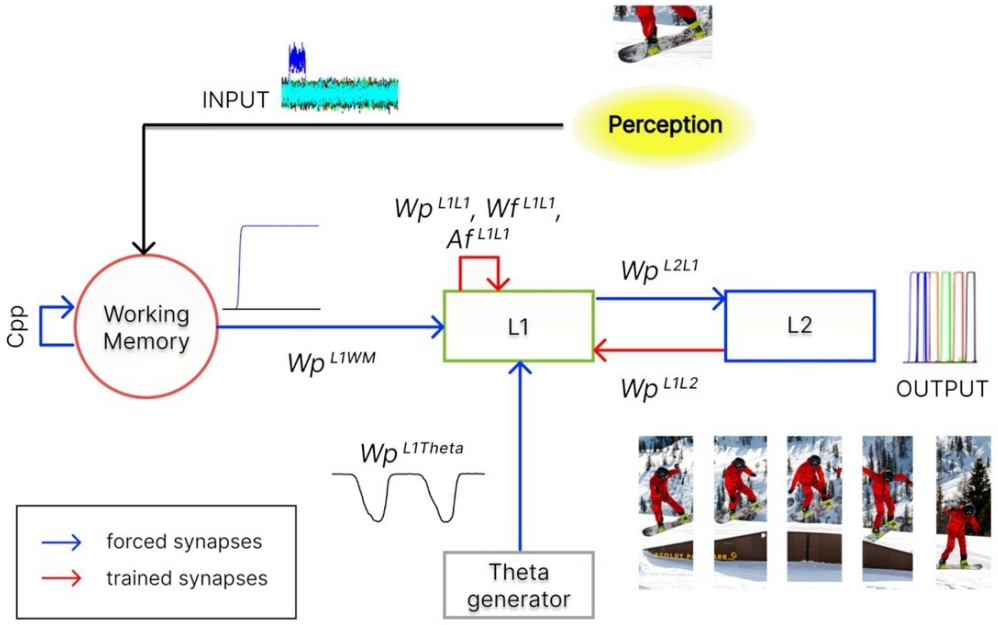

FIGURE 3.2: Organization of the computational areas and their connections for the retrieval of a memorized episodic sequence [39]. Blue lines refer to fixed weights, while red lines indicate trainable synapses.

episodes. The signals are then passed to L2, producing a clean and ordered output of the features in the gamma frequency-band, exploited by the feedforward connections of W_p^{L2L1} and regulated by the feedback synapses W_p^{L1L2}, from which the stored episodic sequence – the snowboarder executing a freestyle trick – is easily acquired.
This system implements properly the retrieval of a temporal sequence, but it is unable to explain its encoding. How can we memorize a series of events and orderly establish the relations between the different features?

3.1.2 Encoding Phase

In this model, the encoding phase needs to be performed before and separately from the retrieval phase. What should be accomplished in this process is the training of the non-fixed weights (W_p^{L1L1}, W_f^{L1L1}, A_f^{L1L1}, and W_p^{L1L2}) with respect to the presented features and their order of appearance.
In this simulation, a total of 75 features is employed: three temporal sequences are object of study; each temporal sequence is constituted by five distinct episodes, and each episode is described by either four, five, or six individual features. To make the sequences comparable during the testing of the model, each ordered episode, from position one to five, is described by the same number of features in all of the chosen sequences (the first episode has always four features, the second always six, and so on).

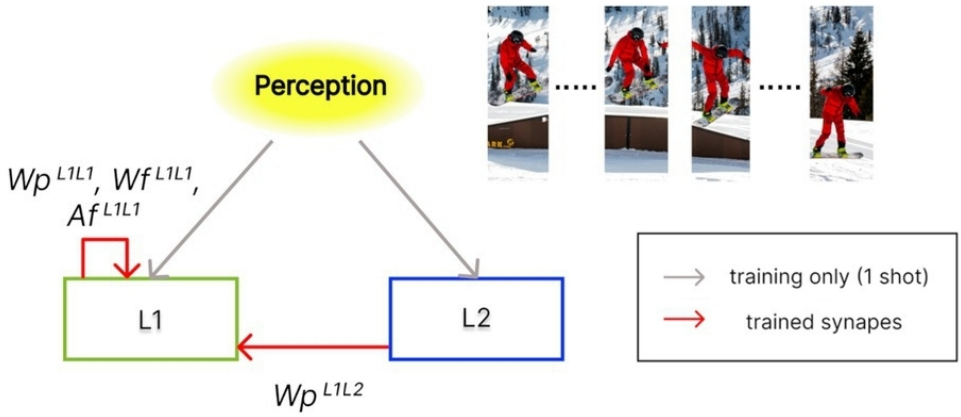

FIGURE 3.3: Representation of the network used during encoding. Grey lines account for direct training of L1 and L2 from the perceptual acknowledgement of episodes [39].

Another point to be reported concerns the presence or absence of commonalities between the features of the different temporal sequences. In most cases, due to sparse representation at the level of the dentate gyrus, features are extracted orthogonally to each other, thus coding only for a specific episode [41]. Despite this, it is not implausible that a few features are shared between distinct episodic events, even if they belong to different temporal sequences. Thankfully, this last case of shared features is still replicable by the model without impairing its functionality, causing acceptable variations in the results from the original hypothesis of orthogonal features.
The learning mechanism selected for the encoding of episodic memory follows a Hebbian rule for glutamatergic weights (W_p^{L1L1}, W_f^{L1L1}, W_p^{L1L2}), and an anti-Hebbian rule for fast desynchronizing synapses (A_f^{L1L1}). The Hebbian principle states that neurons that fire together, wire together. Of course, the principle gets reversed in the case of anti-Hebbian learning, in which neurons firing simultaneously see their synaptic connections suppressed.
As already presented in Figure 1.3, and as hypothesised in this model, connections from EC toward CA3 and CA1 are potentiated during encoding, while interconnections between CA3 and CA1 lose their prominence [17]. The network for encoding can thus be simplified by implementing direct connections from perception toward L1 and L2 separately, with no need of simulating activity by neither the Theta generator nor WM. The resultant system is shown in Figure 3.3.
Computationally, the training is simulated by presenting all the features accounting for an episode to both pyramidal and fast inhibitory subpopulations of L1 and L2, for a total duration of 250ms. Temporal coherence between the two layers is maintained by presenting each episode first to layer L1, then to L2, so that the current (L1) and the previous (L2) episodes are simultaneously

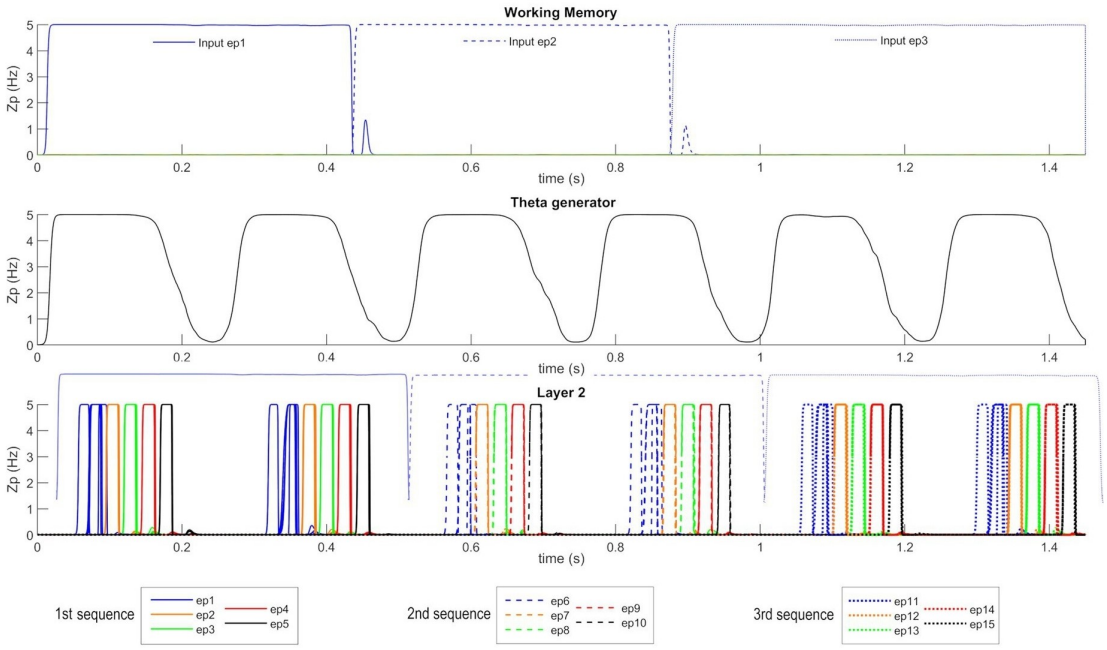

FIGURE 3.4: Results of the retrieval phase for all three temporal sequences using orthogonal features. Pyramidal outputs are plotted for WM, Theta generator and L2 [39].

processed; to apply this, the first episode passed to L2, as well as the last of L1, are provided as null. The training is one-shot: each episode only appears once for both layers.
Synaptic plasticity is simulated through the Hebbian/anti-Hebbian mechanisms, then the obtained weights are normalized based on the amount of features coding for each episode, ideally allocating the same number of synaptic connections per episode without regard of the features implied. This operation is performed so that a higher/lower number of features is not related with stronger/weaker synaptic activation.

3.1.3 Results

After the encoding phase, the theta-gamma coupling neural mass model was tested in its retrieval capability, for all the three temporal sequences. The first results considered orthogonal features, each one only appearing once and coding for a single episode. This case was more linear in the outputs obtained, and easier to interpret with respect to the results after the involvement of shared features.
In Figure 3.4, pyramidal signals from WM, Theta generator, and L2 units, are reported. Theta waves, produced at a frequency of 4Hz, shape the occurrence of gamma waves coupled features. Each episodic sequence presents the same colour appearance (blue, orange, green, red, and black), and is distinguished by the line style, continuous, dashed, or dotted, respectively.

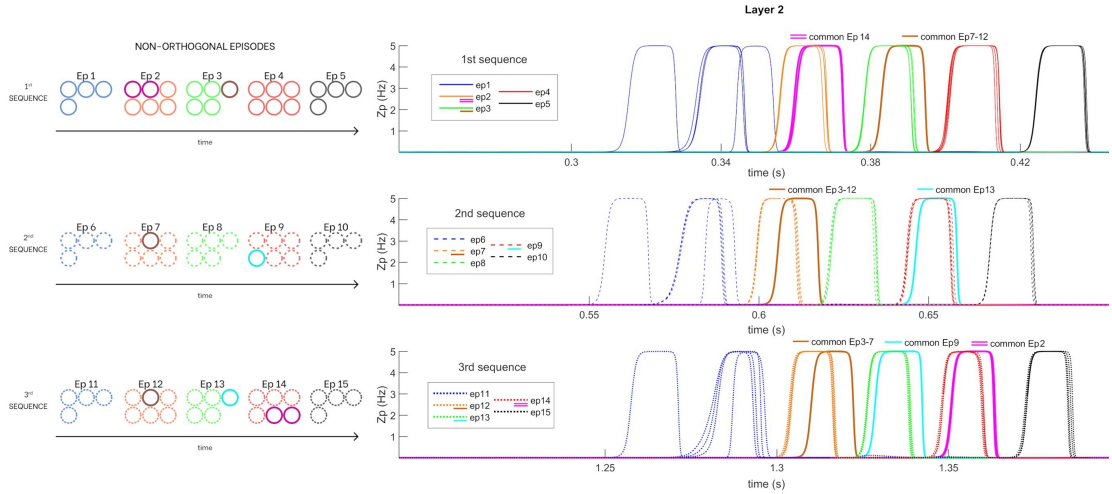

FIGURE 3.5: Retrieval phase L2 outputs admitting shared features, explicited on the left for each episode [39].

After a small delay from the beginning of each theta cycle, all the features coding for the episodes of the specific temporal sequence are activated, starting from the one stored in the working memory – in this case, the first feature of the first episode, for each sequence.
L1 outputs are of similar entity, happening slightly earlier than L2, and presenting a noisier behaviour.
The introduction of shared features and their impact on L2 outputs are presented in Figure 3.5. The major difference from the orthogonal case is the presence of a partial delay in the retrieval of features shared between two or more episodes. Furthermore, the extent of such delay seems related with the amount of different episodes each shared feature belongs to. In fact, it can be harder for a feature to be responsive if its training has involved more than one episode, somehow distributing its synaptic connections in a wider area, with the overall result of a decreased excitability.

3.2 Acetylcholine Model

After the brief presentation of the past model accounting for the theta-gamma entrainment hypothesis, a new neural mass model, explicating the effects of acetylcholine, is hereinafter described.
The most intriguing advancement pursued in this work is the thoroughly assessment of both retrieval and encoding phases in the same simulation. This goal proceeds in parallel with the scientific evidence [17, 42], claiming that high levels of ACh promote episodic encoding, that lower presence of the neurotransmitter is related with the retrieval of experimented events, and that hippocampal ACh levels are regulated by the medial septum and the ventral diagonal band of Broca (MS-VDB).

Most attention will be given to high-ACh theta periods, such as the one occurring during active wakefulness or REM sleep. Additional conditions will be discussed in the next chapter.

3.2.1 The Model

The current neural mass model, accounting for the roles of ACh, presents the same subpopulations and internal connections of the one just mentioned for the simulation of the theta-gamma coupling, except for the MS-VDB computational area, previously referred to as Theta Generator.
This area is modified with the insertion of a new cholinergic subpopulation, modulating the dynamics of pre-synaptic cholinergic neurons. A first order differential equation is chosen to address ACh release towards the hippocampal region CA3. This leads to the addition of a new equation in MS-VDB:

$$\dot{y_c}(t) = \omega_c(\ \mathrm{Sigm}[y_P - C_{cf} y_f(t)] - y_c(t)) \tag{3.1}$$

with y_P the pyramidal noise received at the level of MS-VDB, and c the subscript for the cholinergic subpopulation.
This model is non-variational, and the sigmoid function chosen, which is the same as the model for theta-gamma coupling, is described by:

$$\mathrm{Sigm}[v] = \frac{2e_0}{1 + \mathrm{e}^{-r(v - s_0)}} \tag{3.2}$$

Only a portion of the released ACh successfully binds with the cholinergic receptors; this fraction is calculated time instant after time instant by Hill's equation [43], definable for acetylcholine as:

$$\mathrm{ACh}(t) = \mathrm{ACh}_0 + \frac{y_c(t - T_{\mathrm{ach}})^{\,n_{\mathrm{ach}}}}{k_{\mathrm{ach}}{}^{n_{\mathrm{ach}}} + y_c(t - T_{\mathrm{ach}})^{\,n_{\mathrm{ach}}}} \tag{3.3}$$

Here, Hill's equation is reported in its general form. For the current model, both the parameters accounting for the basal acetylcholine level ACh_0 and the time delay T_{ach} are maintained at zero. The first choice was made in order to keep the ratio of ACh between 0 and 1; for what regards T_{ach}, the time delay was not needed, since delays are introduced later in the model. The remaining parameters, the constant k_{ach} and the exponent n_{ach}, were selected to obtain a realistic response curve, matching biological evidence [44, 45].
At this point, the fraction of receptors bounded by ACh is employed to regulate episodic learning: acting as a coefficient, it linearly modifies the amount of synaptic changes encoded in the trainable weights (Equation 3.4), as well as the direct input connections towards the units L1 and L2 (Equation 3.5), in this way:

$$W_i(t + \Delta t) = W_i(t) + \mathrm{ACh}(t) \cdot \gamma_i \cdot (\mathrm{YX})_i \cdot \Delta W_i \tag{3.4}$$

$$\begin{aligned} E_l(t) &= \mathrm{IN}_l(t) \cdot \mathrm{ACh}(t) \cdot \mathrm{w}_E \\ I_l(t) &= \mathrm{IN}_l(t) \cdot \mathrm{ACh}(t) \cdot \mathrm{w}_I \end{aligned} \tag{3.5}$$

The first equation expresses the Hebbian learning implied in the network, with the index i accounting for each trainable weight, γ the learning rate, Y and X the post- and pre-synaptic activation, and ΔW the array of the differences between the maximal threshold and the weights themselves. The second equation reports the evaluation of the pyramidal (E) and fast inhibitory (I) input signal, weighted by the bounded ACh fraction and a coefficient w, this time with index l indicating either level L1 or L2.
Furthermore, the value resulting from Hill's equation correlates inversely (multiplicative factor 1 - ACh) with the connectivity signals exploited during retrieval, influencing all the computational units involved.
Thanks to this simple approach, the theta waves generated in the medial septum are able to control the release of ACh – high values during troughs, low presence during peaks of theta cycle – and the prominence of this neurotransmitter will accordingly affect learning, setting up a distinct environment for the implementation of encoding and retrieval.

3.2.2 Results

Pyramidal average spike density is simulated for the four computational regions. The ACh rate of absorption is also reported, addressing the encoding of the proposed episodes. The simulations obtained are able to explain both the retrieval and the encoding phases, functioning also in the presence of shared features.
The temporal sequences are of the same type as the ones proposed in the previous model for the theta-gamma coupling, with a total of 75 features, 25 for each sequence, and either 4, 5, or 6, for each episode.
In Figure 3.6, the encoding of the first temporal sequence is reported. Each episode of the overall sequence is presented in temporal order, first in Layer 1 and then in layer 2 (except for the last episode, not provided to L2), by activating all their features at once for 250ms. These periods are identifiable in the figure by the rectangles drawn during high ACh phases, and simulate the incoming signals from the entorhinal cortex. Alternatively to the encoding portions, the retrieval of the progressively memorized episodes is displayed during the low ACh phases, triggered by the feature stored in the working memory. At the end of the training, both layers are able to recover the correct sequence of episodes.
Due to the structure of the model, the area L1 presents a slightly noisier and squared profile with respect to the regular and round shape of L2. Another difference concerns the retrieval of the first and the second episode of each sequence: the feature stored in WM is re-evoked in L1 just between the brief inter-episodic interval. This activation is then transferred to L2; here, however, it appears

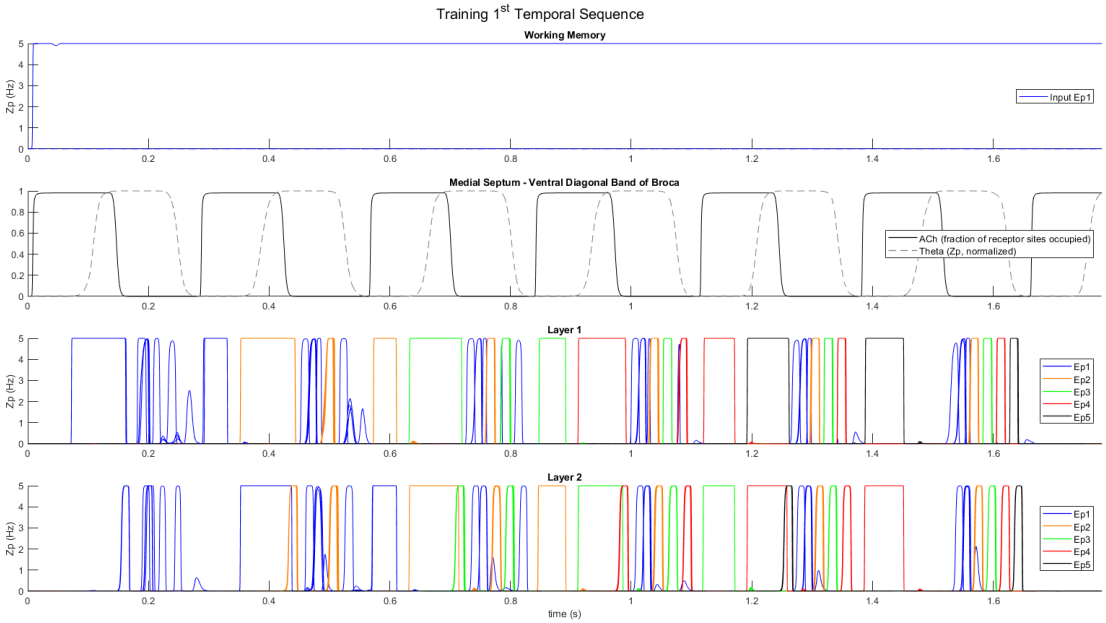

FIGURE 3.6: Training and retrieval of the first temporal sequence.

confined inside the regular gamma cycle of the following episode (which is represented in orange in the figures), although with diminished amplitude. The strength of the introduction of ACh regulation in this neural mass model is fully evident in Figure 3.7: the second temporal sequence, sequentially provided by the entorhinal cortex to CA3 (L1) and CA1 (L2), is accurately encoded during the retrieval of the previously trained one, promoted by a cue maintained in WM. This mechanism functionally imply that learning and recalling operate in unison,

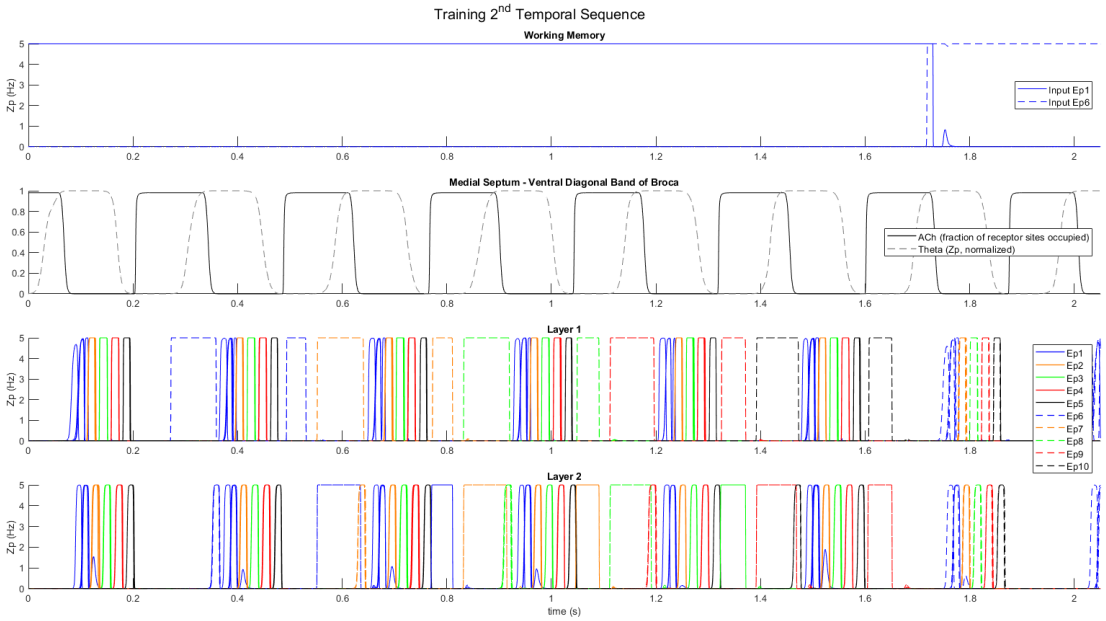

FIGURE 3.7: Training of the second temporal sequence (dashed line) and simultaneous retrieval of the first sequence (continuous line).

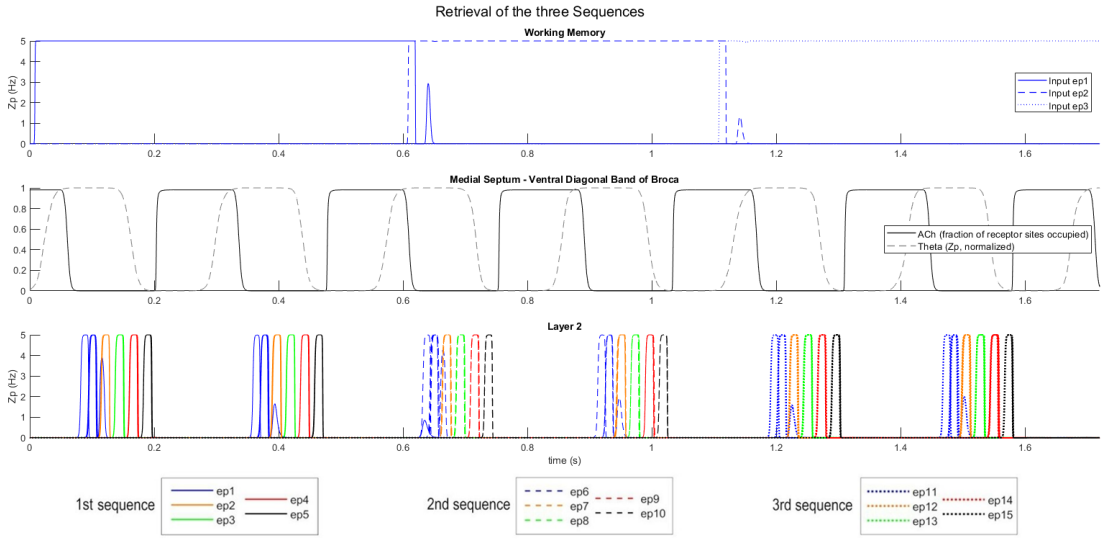

FIGURE 3.8: The three temporal sequences are correctly retrieved.

at least for what regards episodic information, as proposed in [42, 46]. Clearly, when the working memory shifts its focus to a new feature of episode number six (the first of the second temporal sequence), the recently learned sequence is correctly retrieved as expected.

This model was tested on three different episodic sequences, each receiving the same procedure of encoding. The retrieval of the proposed sequences is presented in Figure 3.8, where all the gamma cycles are distinctly visible, from the initial peak of the feature held in WM, to the ordered reinstatement of the memorized episodes.

Notably, the frequency of the theta cycle, here kept at about 4Hz, strongly impacts the amount of information that each cycle is able to carry. Lower theta frequency could allow for the retrieval of more than five episodes, while a faster one would instead decrease the duration of the retrieval phases, setting the recallable episodes to four or even less.

Despite the hurdles and risks of human deep-brain analysis, hippocampal theta frequency and its variability could explain (or be related to) interpersonal and intrapersonal differences in behaviour, showing potential for future research.

A last consideration must be made in the case of shared features, highlighted in Figure 3.9. The differences are not too far from Figure 3.5, accounting for the previous theta-gamma coupling model: the presence of common features between separate episodes modestly affects the retrieval phase, introducing small delays in the activation of the shared components. A notable change introduced in the ACh model was the real-time normalization of the synaptic connections, previously performed exclusively at the end of the encoding. This variation negatively affected the robustness of the shared features, especially the ones coding for more than two sequences (such as the brown one in the figure). Indeed, the spared orthogonal features are much more resistant to variations in

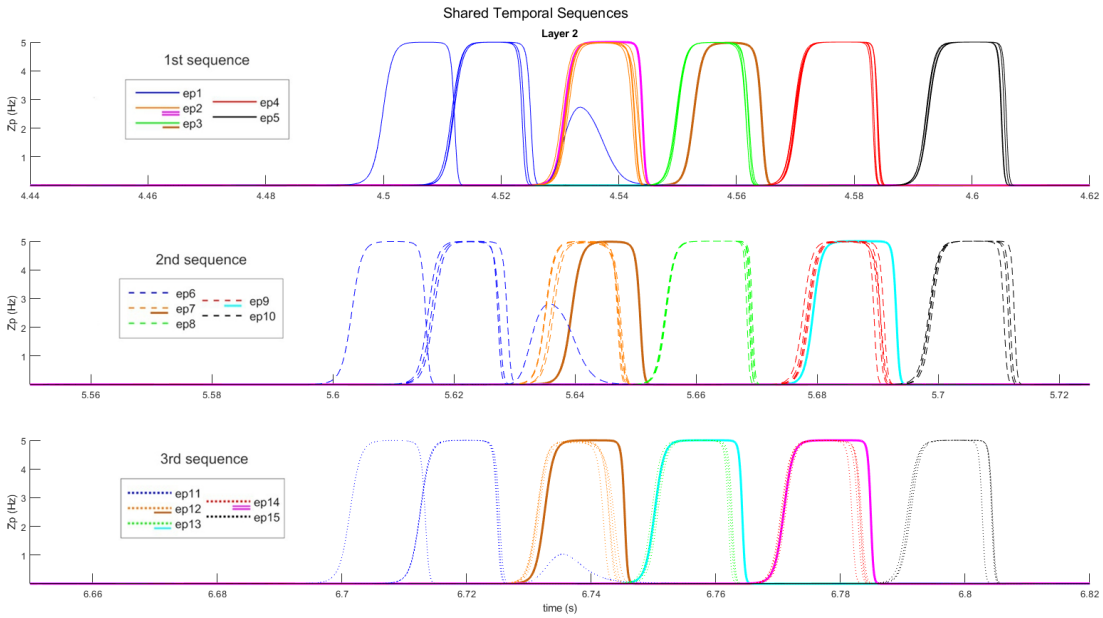

FIGURE 3.9: Shared features highlighted during retrieval phase for all temporal sequences.

the model parameters with respect to the shared ones, and are able to elicit the recall of the subsequent episodes of the sequence with no major issues.
Robustness and sensitivity analysis will be therefore performed on this model in the case of orthogonal features, assuming for a perfectly sparse representation of each episode, keeping in mind that a minor presence of commonalities will neither hinder the encoding nor the retrieval phases up to an irremediable level.

Chapter 4

Model Analysis

In order to acquire quantitative results of the established neural mass model and identify possible flaws or problems in the choice of the parameters or in the structure of the model itself, robustness and sensitivity analyses were performed. The former aims to verify the retrievability of the memorized sequences in the default setting, estimating the range of parametric variations the model is able to withstand without incurring in damaged episodic recovery. At the same time, the latter tries to study the actual effects of such changes to improve the operative knowledge of the whole network, with solutions exploitable for adjusting the model in response to simulated clinical anomalies or unoptimal behaviour.

4.1 Robustness Analysis

The first step in evaluating the accuracy of the developed ACh-mediated neural mass model for episodic memory is to decide what defines a "good" output, i.e. what needs to be achieved by the model to label its result as correct. For this purpose, both encoding and retrieval underwent a thorough assessment, and quantitative values were extracted to estimate the overall model performance.
The examination involved separately the first and the second sequences. The aim was firstly to test the network response to the learning and recalling of a new sequence starting from scratch (as proposed in Figure 3.6); the subsequent goal was to understand how that response changed during the encoding of a second sequence, happening concurrently with the retrieval of the already trained one (reported in Figure 3.7).
The incidence of the random input noise was attenuated by running multiple simulations and executing the arithmetic mean of the count of the correctly retrieved sequences, as well as of the weights and statistical values obtained from each one. The number of iterations chosen was of 20 total simulations, enough for a good estimation of the results. On top of that, the starting time point for the encoding phase was also randomly modified (in a range of $\pm$100ms) during each iteration, so that the beginning of the presentation of the episodic

sequence was not impactful for the purposes of the evaluation. A time range of $\pm$200ms was also tested, but did not introduce pivotal changes in the analysis.
The statistical values inspected during the sensitivity analysis were: (i) the duty cycle (threshold at the 80^{th} percentile) of the pyramidal subpopulation of MS-VDB, generator of the theta waves; (ii) the duty cycle (same percentile) of its cholinergic subpopulation, accounting for ACh release; (iii) the cholinergic firing rate, assessing for the theta frequency; (iv) the average of the fraction of ACh bound to cholinergic receptors, obtained by Hill's equation; (v) the saturation point of ACh, evaluated as the maximum fractional value assumed during the simulation.
Together with these results, numerical properties were extracted to assess the encoding and retrieval capacities of the network: the retrieval of an episode was established as correct whenever the totality of the features reached the threshold of 90% within the correct gamma cycle, before the occurrence of any other feature belonging to different episodes. Enough time was provided to each simulation so that the sequence in study could be recovered about six times after the completion of its training, making for an ideal total of 120 possible retrievals. The results were reported in ratios (from 0 to 1), explicating the percentage of correct recalls separately for each episode.
For what concerns the encoding, the averages of the absolute values of the non-zero weights were obtained for each episode of the temporal sequence under analysis. These values are not significant per se, but acquire importance in their relation with the training values of the second sequence. The proposed weights for the new sequence are in fact calculated by dividing each element with the respective value produced in the first training, making such results more readable and easier to understand. Of course, the obtained weights are not intended to be exactly equal for the two sequences, since this involves different features and synapses, but a certain degree of similarity is certainly expected.

4.1.1 First Sequence

In Table 4.1, results about the first temporal sequence are reported. The encoding outputs are presented in their mean value. The normalization executed during training had the purpose of allocating the same number of synapses for all the episodes regardless of the amount of features. This step is mainly visible in W_p^{L1L1} and W_f^{L1L1}, where the second and fourth episodes, being the longest (composed of six features instead of the four of episode 1 and 2, and the five features of episode 3), appear with reduced weights overall. Notably, the value of the fifth episode for W_p^{L1L2} is null, due to the nature of the network and the structure of the training.
There is not much to say for the retrieval, which reports a perfect score for the first temporal sequence as expected.
The statistical parameters presented verify the theta behaviour of ACh binding,

with frequency of approximately 4Hz, and affirm the high saturation of ACh, stable at 98%. The duty cycles are all slightly inferior to 0.5, the cholinergic value being lower than the pyramidal one, while the average fraction of bound ACh settles at 46%. These default values describe the normal functioning of the neural mass network, and are thought to be compared with changes in the parameters for the analysis of sensitivity.

4.1.2 Second Sequence

One of the main aims of this model is the achievement of simultaneous encoding and retrieval of separate sequences. This goal is assessed in the robustness analysis via the presentation of one feature of the first sequence (already correctly encoded) to the WM, while the entorhinal cortex proceeds to send the training information about the second sequence to L1 and L2. After the encoding phase, the input to the WM is changed into a feature of the first episode in the second sequence just encoded, and its recalling ability is now tested. The output of such

Robustness Analysis - 1st Sequence

Encoding - Absolute Values

	1st ep.	2nd ep.	3rd ep.	4th ep.	5th ep.
Wp_L1L1	126.62	104.00	125.66	104.00	127.57
Wf_L1L1	9.19	6.12	7.65	6.12	9.23
Af_L1L1	0.76	0.76	0.76	0.76	0.75
Wp_L1L2	64.63	64.39	64.90	65.32	0.00

Statistics

Duty Cycle Pyramidal	0.4657
Duty Cycle Cholinergic	0.4328
ACh Frequency (Hz)	3.9413
ACh Average	0.4619
ACh Saturation	0.9808

Retrieval - Rates

	1st ep.	2nd ep.	3rd ep.	4th ep.	5th ep.
Seq. 1	1.00	1.00	1.00	1.00	1.00

TABLE 4.1: Values obtained in the robustness analysis regarding the encoding and retrieval of the first temporal sequence.

Robustness Analysis - 2nd Sequence

Encoding - Rates

	1st ep.	2nd ep.	3rd ep.	4th ep.	5th ep.
Wp_L1L1	1.012	0.981	0.999	0.981	1.003
Wf_L1L1	1.010	0.981	0.981	0.981	1.005
Af_L1L1	0.989	0.986	0.987	0.986	0.991
Wp_L1L2	1.016	1.023	1.018	1.004	0.00

Statistics

Duty Cycle Pyramidal	0.4634
Duty Cycle Cholinergic	0.4342
ACh Frequency (Hz)	3.8912
ACh Average	0.4638
ACh Saturation	0.9808

Retrieval - Rates

	1st ep.	2nd ep.	3rd ep.	4th ep.	5th ep.
Seq. 1	1.00	1.00	1.00	1.00	0.9875
Seq. 2	1.00	1.00	1.00	1.00	1.00

TABLE 4.2: Robustness analysis results assessing the encoding and retrieval of the second temporal sequence, and the inter-training retrieval of the previously encoded first sequence.

Robustness Analysis - ACh Parameters

Parameter	Lower Limit	Default Value	Higher Limit	
σ	-	5	30	
k_ach	0.28	0.7	2.20	
n_ach	0.92	2	-	
ω_c	195	300	-	
C_MS,cf	0.69	0.9	4.80	× 67.5
C_MS,fp	0.89	1	1.95	× 81

TABLE 4.3: Limit values for ACh-related parameters, allowing for a retrieval of at least 90% for all episodes of the first and second temporal sequences, during simultaneous encoding and retrieval.

process is comparable to the one reported in Figure 3.7.
The quality of the encoding, as explained before, is provided as ratios related to the first sequence's training values, while the recovering assessment procedures remain unchanged.
The results obtained are shown in Table 4.2: starting from the statistical values, no important variations occur; all the parameters present numbers analogous to the previous test. The encoding values of the secondly trained sequence are slightly different (around $\pm 2\%$) from the ones seen in Table 4.1, but these changes do not hinder the encoding phase. As it will be apparent in the following paragraphs, the network is able to withstand variations in weights of about 20% before incurring in encoding damages. The retrieval capacity of the network is satisfactory even for the second sequence but is not able to reach a perfect score during the simultaneous encoding and retrieval of the second and first temporal sequences: in particular, the last episode is not retrieved in its totalities of occurrences. This rare event (taking place only in one/two instances among the 120 ones simulated) might happen due to the smaller gap available to execute the recovering; the retrieval time interval in fact undergoes a minimal but not negligible compression between the two saturated rectangles of the encoding phase.
From these elements, it is safe to state that the network is able to produce good encoding and retrieval of multiple sequences, even when the two phases are operating concomitantly.
A selection of ACh response modulating parameters – treated in detail in the next section – is proposed in Table 4.3, along with their default value and lower/upper extremes of functioning. The parameters are reported together with the variance of the noise σ (actually computed as $\sqrt{\sigma/\Delta t}$, Δt being the time step duration). The boundaries of the working intervals were iteratively found to assure a retrieval of at least 90% for all episodes; this method was conducted during the case of simultaneous encoding and retrieval, for both the temporal sequences involved.
These numerical results are presented to give an idea of the resilience of the

network, operating properly even in non-optimal conditions, and remaining consistent, or 'robust', in a wide range of possible parametric values. Some of the exposed parameters are more prone to failure at lower values, such as the connectivity constants and the cholinergic time constant, which needs to remain high to ensure fast ACh dynamic. The dashed lines instead indicates no limit for the specific parameter, thus meaning 0 for the lower limit and infinite for the higher limit.
Nevertheless, numbers are not always the best cues when explanation is taken into account. In the next analysis, a more deep inspection of what is causing the found results will be performed, producing new insights and knowledge about the thorough functioning of the proposed neural mass model.

4.2 Sensitivity Analysis

After the functioning assessment verified through the robustness analysis, a second test was conducted to encompass the actual effects of parametric changes on the model. Due to the high number of parameters implemented, a complete description of the events taking place during the modification of such values would be burdensome and ineffective. Instead, the focus was shifted to the behaviour of ACh in the network, being this neurotransmitter the main new aspect of the current model.
Three characteristics were selected: the saturation of the bounded ACh, its dynamics, and the cholinergic duty cycle, guiding ACh release. For each of these elements, the most impactful parameters were identified and investigated.
The testing procedures were the same as the previous ones used in the evaluation of the robustness, thus 20 simulations with default random seed and $\pm$100ms interval for the selection of the encoding starting point. The parameters were stressed until failure occurred, affecting either the retrieval alone, the encoding, or even both phases.

4.2.1 ACh Saturation

One of the most straightforward elements introduced in this model was the evaluation of the bounded ACh by means of Hill's equation (as proposed in Equation 3.3). Here, the contribution to the output fraction of cholinergic receptors occupied is simply due to two parameters, namely n_{ach} and k_{ach}. Computationally speaking, the first parameter modifies the sigmoid-like exponential behaviour, thus the steepness of the slope, while the second horizontally translates the 50^{th} percentile threshold of the function, consequently modifying the amount of neurotransmitter required for reaching a higher saturation. Biological evidence from neuroscientific literature suggest that the value of the exponential factor n for acetylcholine should range between 1.7 to 2.3 [47, 48]; experimental results

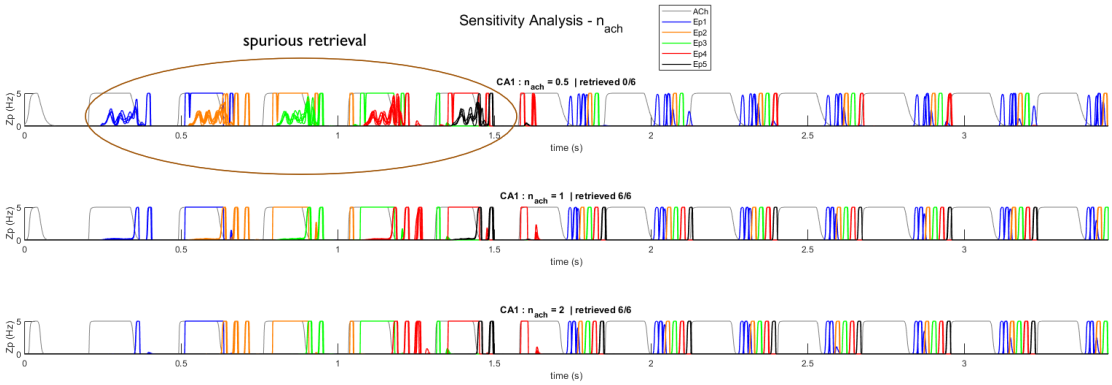

FIGURE 4.1: Plots obtained with three different values of n_{ach} (default: $n_{\text{ach}} = 2$). ACh levels are normalized for clarity; spurious retrieval is highlighted for low n_{ach} values.

with this model affirm that a good network functioning is obtained with $n_{\text{ach}} = 2$ and $k_{\text{ach}} = 0.7$.

ACh saturation is strictly related with the encoding quality: a higher saturation produces a stronger Hebbian activation, allowing for better and faster training. Lower binding of ACh might instead damage the ability of the network to discriminate between encoding and retrieval, resulting in poor training quality and in spurious recalls of the current episode in CA3 during the encoding phase.

Variations in these two parameters were investigated throughout the training of the first temporal sequence, and the acquired plots are shown in Figure 4.1 for n_{ach} and in Figure 4.2 for k_{ach}.

The exponential parameter of Hill's equation has a double effect on this model: higher n_{ach} values produce higher ACh saturation and contribute at the same time to faster ACh binding dynamics. This is expected since n identifies the cooperativity of the receptors, therefore using a higher value for n_{ach}, with unchanged cholinergic pre-synaptic activation, is related with faster and denser post-synaptic potentials.

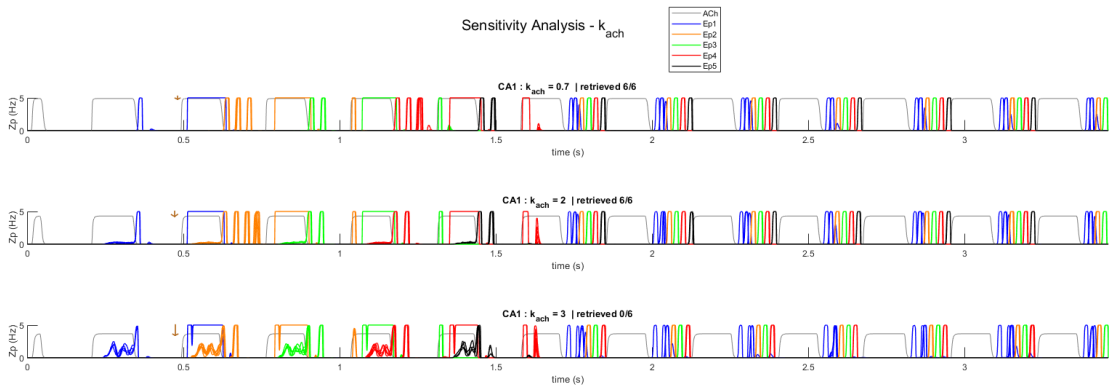

FIGURE 4.2: Three different values of k_{ach} are studied (default: $k_{\text{ach}} = 0.7$). Here the signals for ACh binding are not normalized, in order to highlight the decrease in saturation.

Sensitivity Analysis - n_ach

Statistics

Value **n_ach**	0.5	1	2	3	4
Duty Cycle Pyramidal	0.4657	0.4657	0.4657	0.4657	0.4657
Duty Cycle Cholinergic	0.4328	0.4328	0.4328	0.4328	0.4328
ACh Frequency (Hz)	3.9412	3.9412	3.9413	3.9412	3.9412
ACh Average	0.3654	0.4189	0.4619	0.4696	0.4709
ACh Saturation	0.7277	0.8772	0.9808	0.9973	0.9996

Failure Case: **n_ach** = 0.5

Encoding - Rates

	1st ep.	2nd ep.	3rd ep.	4th ep.	5th ep.
Wp_L1L1	0.807	0.993	0.817	0.994	0.805
Wf_L1L1	0.867	1.297	1.045	1.295	0.867
Af_L1L1	0.742	0.747	0.744	0.747	0.741
Wp_L1L2	0.723	0.722	0.719	0.715	0.00

Retrieval - Rates

	1st ep.	2nd ep.	3rd ep.	4th ep.	5th ep.
Seq. 1	0.6583	0.9917	0.9333	0.4000	0.0083

TABLE 4.4: Changes in statistical parameters by variations of n_{ach} with highlighted ACh saturation, and failure case with encoding and retrieval results – the highlighted retrieved values are not acceptable.

Sensitivity Analysis - k_ach

Statistics

Value **k_ach**	0.7	1.5	2	2.5	3
Duty Cycle Pyramidal	0.4657	0.4657	0.4657	0.4657	0.4657
Duty Cycle Cholinergic	0.4328	0.4328	0.4328	0.4328	0.4328
ACh Frequency (Hz)	3.9413	3.9413	3.9412	3.9412	3.9412
ACh Average	0.4619	0.4162	0.3854	0.3538	0.3223
ACh Saturation	0.9808	0.9174	0.8621	0.8000	0.7353

Failure Case: **k_ach** = 3

Encoding - Rates

	1st ep.	2nd ep.	3rd ep.	4th ep.	5th ep.
Wp_L1L1	0.761	0.929	0.761	0.926	0.750
Wf_L1L1	0.832	1.250	0.995	1.244	0.821
Af_L1L1	0.702	0.705	0.704	0.706	0.704
Wp_L1L2	0.670	0.665	0.664	0.658	0.00

Retrieval - Rates

	1st ep.	2nd ep.	3rd ep.	4th ep.	5th ep.
Seq. 1	0.5183	0.8933	0.8567	0.6267	0.2167

TABLE 4.5: Sensitivity analysis executed on the parameter k_{ach} with highlighted elements of interest.

Spurious retrieval occurs for n_{ach} values lower than one, due to a decrease in saturation. The features partially retrieved during the encoding in CA1 (L2) are the ones being trained in region CA3 (L1), as can be seen from the image. Of course, this event causes damages in the learning of the temporal sequence, slowing down the retrieval process and making harder for the network to reach the last episode, which is the reason of the null score (0 out of 6) in figure for n_{ach} value of 0.5 (worsened by the additional effect on ACh dynamics, explained below in more details).

The parameter k_{ach} only affects the level of ACh saturation. Spurious retrieval is evident for lower values of saturation, while ACh dynamics remains practically untouched.

Quantitative results were acquired to justify the qualitative evidence, and are here summarized in the two proposed tables for n_{ach} (Table 4.4) and k_{ach} (Table 4.5).

The main elements affected by each of the two parameters are highlighted with yellow-coloured lines, in this case ACh saturation (which automatically modifies the average ACh), and the retrieval accuracy of the first sequence. The encoding rates are evaluated in proportion to the training values obtained for the first temporal sequence with default parameters.

4.2.2 ACh Dynamics

As previously reported, a first effect on ACh binding dynamics can find explanation in the parameter n_{ach}, playing a role in the speed of the exponential fall for each theta cycle. A similar, more uniform event takes instead place by varying the inverse of the time constant ω_c, which organically modulates the dynamics of the ACh binding curve. Higher pulsation (lower time constant) is related to faster linking with cholinergic receptors, and the opposite is of course true for lower pulsation (higher time constant).
ACh binding dynamics affects particularly the retrieval of the given sequences: a slower ACh curve directly implies that the temporal passage between the encoding and retrieval phases is stretched, actually stealing a percentage of the time that was intended for the episodic recalling. The result of this event is a damaged retrieval phase, which is too short to sequentially remember all the stored episodes, while the encoding is performed as usual. The best place to assess this occurrence is the double-sequence case, especially during the retrieval periods between the training intervals, where the already learned first sequence is recalled within two encoding phases of the second sequence.
In Figure 4.3 the simulation is run for three values of ω_c, and the amount of completely retrieved sequences is counted. As can be seen from the middle plot ($\omega_c = 150$) the inter-training sequences are tougher to be recalled in their totality, and the last episode seldom compares. This hardship might eventually present in unlucky simulations with default values, as one occurs in the third plot ($\omega_c = 300$) where one of the black episodes does not reach the imposed threshold at 90%, scoring 13 out of 14 correctly recalled sequences.
Quantitative values are reported for completeness in Table 4.6. The main change brought by ω_c is the variation of the mean ACh fraction bound to the receptors, inversely related to the parameter. The encoding of the second sequence, as outlined previously, is basically perfect, while the last episode of the first sequence struggles to emerge, stopping at the 65% of retrievability.
The value chosen for the default analysis is of 300Hz, the analogue of a time

Sensitivity Analysis - ω_c

Statistics

Value **ω_c**	50	100	150	200	300
Duty Cycle Pyramidal	0.4634	0.4634	0.4634	0.4634	0.4634
Duty Cycle Cholinergic	0.4342	0.4342	0.4342	0.4342	0.4342
ACh Frequency (Hz)	3.8785	3.8892	3.8914	3.8910	3.8912
ACh Average	0.6094	0.5228	0.4933	0.4785	0.4638
ACh Saturation	0.9803	0.9808	0.9808	0.9808	0.9808

Failure Case: **ω_c** = 150

Encoding - Rates

	1st ep.	2nd ep.	3rd ep.	4th ep.	5th ep.
Wp_L1L1	1.024	1.000	1.013	1.000	1.027
Wf_L1L1	1.007	1.000	1.000	1.000	1.010
Af_L1L1	1.013	1.012	1.012	1.012	1.012
Wp_L1L2	1.041	1.042	1.042	1.042	0.00

Retrieval - Rates

	1st ep.	2nd ep.	3rd ep.	4th ep.	5th ep.
Seq. 1	1.00	1.00	0.9688	0.9625	0.6554
Seq. 2	1.00	1.00	1.00	1.00	0.9917

TABLE 4.6: Sensitivity analysis of ω_c. Mean ACh binding is highlighted, as well as the insufficient retrieval value of the last episode of the first sequence.

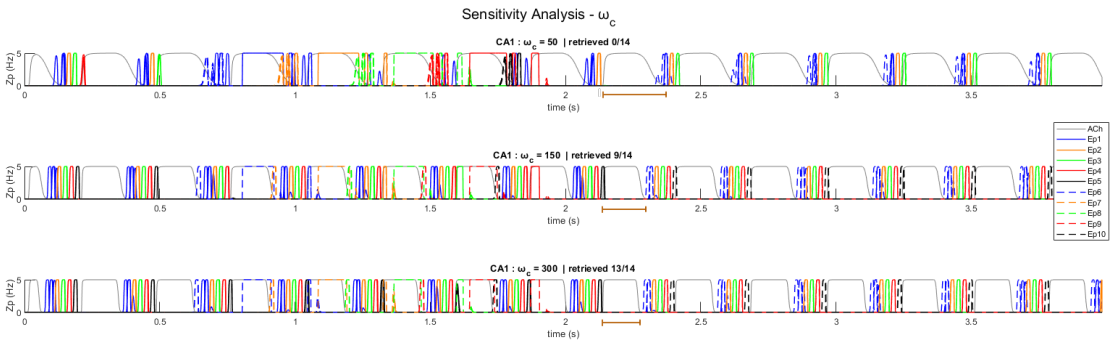

FIGURE 4.3: Different plots obtained while changing ω_c values. In brown, the duration of each ACh binding cycle is qualitatively reported.

constant of slightly more than 3ms. Although this speed remains in a biological range for very fast neurotransmitter release, it is possible to reduce this value without interfering too much with the optimal results obtained by default. Successive works will certify the most neurobiologically accurate number to adopt in neural mass models of this kind, heightening the accuracy of the simulations and widening their applicability to real-case solutions.

4.2.3 Cholinergic Duty Cycle

The duty cycle measurement of the cholinergic neural activity is an optimal resource to estimate the equilibrium between the encoding and retrieval phases. A certain balance is required to allow a simultaneous elaboration of the two processes, and, as a consequence, a specific trade-off must be achieved.
The cholinergic duty cycle, as previously anticipated, is defined as the percentage amount of the ACh-based firing activity in the MS-VDB region able to remain above the 80% of the maximal activation frequency (here limited at 5Hz, therefore setting the duty cycle threshold at 4Hz).
Remembering how the ACh binding signal, obtained from the Hill's equation, determines the encoding portions of the network, it is clear that a higher duty cycle will produce a longer encoding at the expense of the spared retrieval intervals, which instead will see their duration diminished. Conversely, lower cholinergic duty cycles will reduce the overall training time while opening up for greater recalling periods. It is as well ascertained that insufficient encoding intervals will result in a delayed or even incorrect retrieval of the selected episodic sequence due to an imperfect memorization, whereas a scarce recalling time will not allow for the thorough recovering of the features, even if perfectly trained.
Multiple tries were computationally required to find a compromise for such a stalemate, optimizing the parametric functionality of the model change after change, and ultimately establishing a theta-related duty cycle of 46% and a cholinergic one of about 43%.

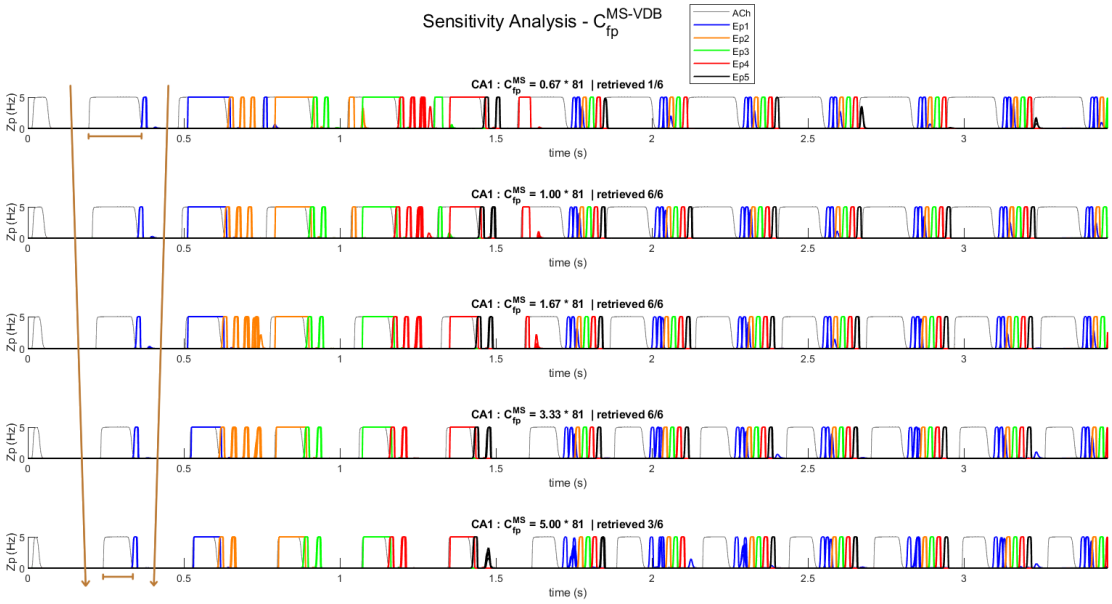

FIGURE 4.4: Plots explaining changes to C_{fp}^{MS} while encoding and retrieving a single sequence. The effect of C_{cf}^{MS} is analogous.

Two are the main parameters that determine the cholinergic duty cycle, in particular two connectivity constants regulating the functioning of the MS-VDB area: C_{fp}^{MS} and C_{cf}^{MS}, being MS the abbreviation of MS-VDB. These two constants affect the signal emerging from the pyramidal toward the fast inhibitory subpopulation, and from the fast inhibitory onto the cholinergic subpopulation, respectively.
Since the effects of such connections on the cholinergic output are relatively comparable, a single graphical representation is provided for C_{fp}^{MS} during the training and later retrieval of the first sequence alone, explicated in Figure 4.4.
The major influence of the constants is evident in the spread of the ACh binding signal, which properly correlates with the extent of the cholinergic duty cycle. Lower values of the connection ruled by C_{fp}^{MS} imply that the fast inhibitory subpopulation gets less and less stimulated by the pyramidal neurons, resulting in

Sensitivity Analysis - C_MS,fp

Statistics

Value **C_MS,fp * 81**	0.67	1.00	1.67	3.33	5
Duty Cycle Pyramidal	0.4634	0.4634	0.4634	0.4634	0.4634
Duty Cycle Cholinergic	0.5132	0.4342	0.3608	0.2809	0.2395
ACh Frequency (Hz)	3.8901	3.8912	3.8950	3.8978	3.8992
ACh Average	0.5445	0.4638	0.3907	0.3119	0.2712
ACh Saturation	0.9808	0.9808	0.9808	0.9808	0.9808

Failure Case: **C_MS,fp** = 3.33 * 81

Encoding - Rates

	1st ep.	2nd ep.	3rd ep.	4th ep.	5th ep.
Wp_L1L1	0.799	0.967	0.815	0.974	0.802
Wf_L1L1	0.856	1.000	0.984	1.000	0.866
Af_L1L1	0.888	0.894	0.891	0.893	0.887
Wp_L1L2	0.719	0.719	0.723	0.725	0.00

Retrieval - Rates

	1st ep.	2nd ep.	3rd ep.	4th ep.	5th ep.
Seq. 1	1.00	1.00	1.00	1.00	1.00
Seq. 2	0.6750	0.9617	0.9517	0.8933	0.7317

TABLE 4.7: Sensitivity analysis of the connectivity constant C_{fp}^{MS}, with failure case exploring low cholinergic duty cycle condition.

Sensitivity Analysis - C_MS,cf

Statistics

C_MS,cf * 67.5	0.37	0.90	3.6
Duty Cycle Pyramidal	0.4634	0.4634	0.4634
Duty Cycle Cholinergic	0.5237	0.4342	0.3595
ACh Frequency (Hz)	3.6429	3.8912	3.8963
ACh Average	0.6568	0.4638	0.3883
ACh Saturation	0.9808	0.9808	0.9808

Failure Case: **C_MS,cf** = 0.37 * 67.5

Encoding - Rates

	1st ep.	2nd ep.	3rd ep.	4th ep.	5th ep.
Wp_L1L1	1.125	1.000	1.016	1.000	1.122
Wf_L1L1	1.077	1.000	1.000	1.000	1.079
Af_L1L1	1.073	1.076	1.075	1.076	1.072
Wp_L1L2	1.184	1.184	1.174	1.194	0.00

Retrieval - Rates

	1st ep.	2nd ep.	3rd ep.	4th ep.	5th ep.
Seq. 1	0.4111	0.4580	0.4092	0.1417	0.0330
Seq. 2	0.8014	0.9124	0.8152	0.2952	0.00

TABLE 4.8: Analysis of C_{cf}^{MS}, reporting this time the failure case of exceedingly high cholinergic duty cycle.

a smaller inhibition and a consequent boost to the cholinergic activity. The same happens for lower C_{cf}^{MS}, where the actual fast inhibitory circuit is weakened in its GABAergic regulation, widening the theta-regulated cholinergic output.
At the two extremities of the figure ($C_{fp}^{\mathrm{MS}} = [0.67; 5] \cdot 81$) the just mentioned unbalance becomes visible in the plots: the first displays too large portions dedicated for encoding, without enough space to allow the recalling of the final episode; the last plot instead features a too short ACh saturation state, resulting in poor encoding and struggling especially in the activation of the initial features.
Numerical values are reported for C_{fp}^{MS} and C_{cf}^{MS} in Table 4.7 and Table 4.8 in the simultaneous encoding and retrieval case, quantitatively expressing the elements just discussed.
Starting with C_{fp}^{MS}, it is plain to see that a higher connectivity constant compacts the cholinergic signal, and directly reduces the mean ACh binding fraction. The effect is a poor encoding of the new sequence, and therefore a damaged retrieval, while the one already trained is perfectly recalled.
The second table presents the two extremes of functioning and the default value in the middle for C_{cf}^{MS}. The focus here is on the extraordinarily lower connectivity case ($C_{cf}^{\mathrm{MS}} = 0.37 \cdot 67.5$), where the encoding is broad and hyper-effective, even exceeding the default values. Unluckily, a flawless training is of no use if no space is given for its effective application. In fact, both the previous sequence and the new one exhibit catastrophic retrievals, predominantly concerning the last episodes.
The absence of a firm inhibition is clearly detrimental for the functionality of the network, and corresponding clinical conditions would require the reestablishment of the inhibitory circuit by potentiating GABAergic neurons in the localized region of interest. Clinical application is in fact one of the aims of neurobiological models, and advancements in this sector, paper after paper, will eventually grant healthcare experts with a powerful medical tool to increase treatment accuracy, reduce clinical costs and hospital stay, and ultimately improve the quality of life

for all people around the globe.
Therefore, how close is this neural mass model to an actual medical implementation? What are its limits, and what are its true capacities?

Chapter 5

Clinical Examples and Conclusions

Defining models by mathematical means and extensively discussing numerical entities might withdraw the attention from the actual pathologies affecting multiple people worldwide, problems that triggered the establishment and improvement of the models themselves.
Acetylcholine is, in fact, a fundamental messenger for multiple reasons, being involved in peripheral muscular contraction, blood pressure regulation, and glandular secretion while acting in the central nervous system as a fast but generally fleeting neurotransmitter in the spinal cord, thalamus, limbic system and cortex, all of this through its nicotinic and muscarinic receptors [15].
Furthermore, the cholinergic participation in episodic memory has been previously discussed [17, 42], stressing its role as a promoter of the encoding process and analogously orchestrating the retrieval in the periods of low ACh, mediated in its rhythm by the MS-VDB activity.
In the next pages, some pathological conditions will be treated by means of the ACh-mediated theta-gamma coupling neural mass model achieved, together with some additional tests regarding quiet waking and slow-wave sleep. The final section will critically expose the limitations of the model to be addressed in future works, completing the dissertation with pros, cons, and a few conclusive words.

5.1 Clinical Cases

The role of ACh in the model has been previously tested and analysed computationally by changing the parametric values of interest. Now that some knowledge has been provided about the area of action of ACh-related parameters, it would be intriguing to change the point of view back into the biological domain and highlight the effects of pathological-like conditions by exploiting this model and its results.
General damages in the transport or production of the neurotransmitter are therefore addressed below in two separate instances, focusing on the impact of

each one on the functionality of episodic memory.

5.1.1 Low Saturation during Encoding

Variations in the presence of inter-synaptic ACh could be due to various reasons: damages could involve pre-synaptic ACh transport, storage and release; the reuptake (recollection of the neurotransmitter by the pre-synaptic neuron) could be scarce or excessive; cholinergic receptors might be present in different types and percentages; and somatic or inherited mutations, restricted or not to the domain of acetylcholine, could disrupt the typical chemical synaptic processes. In this model, the two elements that allow for all these possible changes are the Hill's parameters n_{ach} and k_{ach}, modulating cholinergic release into the fraction of the receptors occupied by ACh. The computational meaning of the parameters has already been discussed, while their biological interpretation is much more subtle, incorporating all mentioned functions into a simple numerical set of an exponent and a constant.
n_{ach} and k_{ach}, while both related to ACh modeling, represent distinct physiological aspects. The n_{ach} exponent relates to the average cooperativity of receptors, thus affecting the sensitivity of the system; whereas the k_{ach} parameter represents an indirect measure of ligand-receptor affinity – a high value of this parameter signifies a low binding rate. The index of cooperativity explains the capacity of the receptors to influence, positively or negatively, future bindings after the first one has occurred, while the dissociation constant k_{ach} explains the ligand concentration required to bind exactly half of the cholinergic receptors.
As it is clear from Chapter 4, both a decrease in n_{ach} and an increase in k_{ach} result in lower ACh binding saturation. This is biologically explainable since a lower cooperativity (lower n_{ach}) and a lower affinity (higher k_{ach}) will similarly hinder the binding of the neurotransmitter.
ACh saturation is especially important during the encoding phase, where the proposed episodes are memorized into sequences. A reduction in the saturation means that fewer neurotransmitter is bound to the cholinergic receptors, which biologically indicates a decrease in postsynaptic firing rate, resulting in reduced neural learning and synaptic strengthening.
This condition is proposed in Figure 5.1 and Figure 5.2 by varying singularly n_{ach} and k_{ach}. The saturation levels achieved during the encoding of the second sequence and its first three retrievals were about 73% for $n_{ach} = 0.5$ and 75% for $k_{ach} = 2.9$. The parameters were reset at their default value at the third second of the simulation, after which three retrieval phases followed, recovering the already stored sequence, and then other four for the new one.
The results are evident: the first sequence is easily retrieved, while the second is not properly memorized, and thus struggles to be recovered. On top of this, the effect of n_{ach} on ACh dynamics can be distinguished for its lower value, reducing the available retrieval time and even worsening the first three recalls of

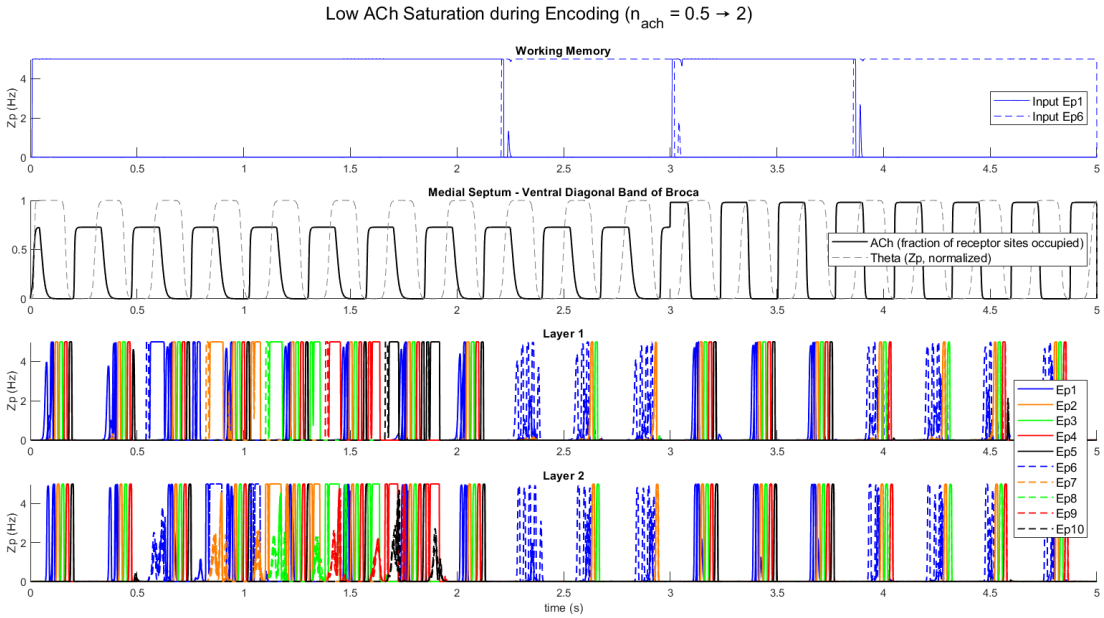

FIGURE 5.1: Results obtained with low n_{ach} during the encoding of the second sequence.

the second sequence. This event does not take place when changing the ligand-receptor affinity, modulated by k_{ach}, where the dynamics is instead preserved. The quality of the encoding of the new sequence can be established in Figure 5.3, where all the trainable weights are reported, feature-by-feature, using a colour map. The left side regards the training of the first sequence, learned previously in normal conditions, while the right portion explains the encoding of the second

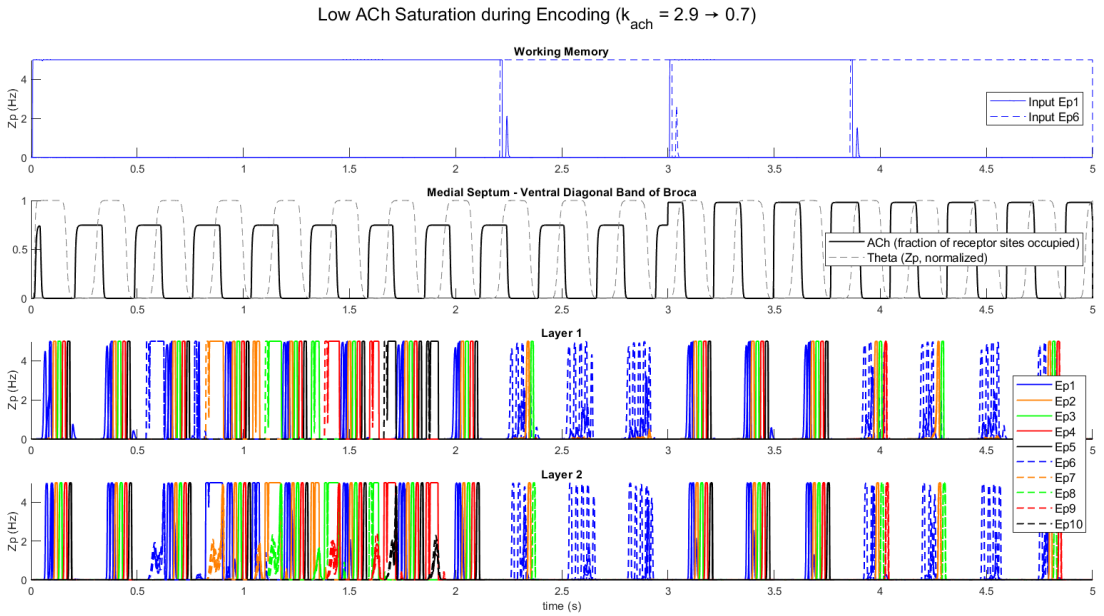

FIGURE 5.2: Plots representing high k_{ach} levels during the encoding in the double-sequence case.

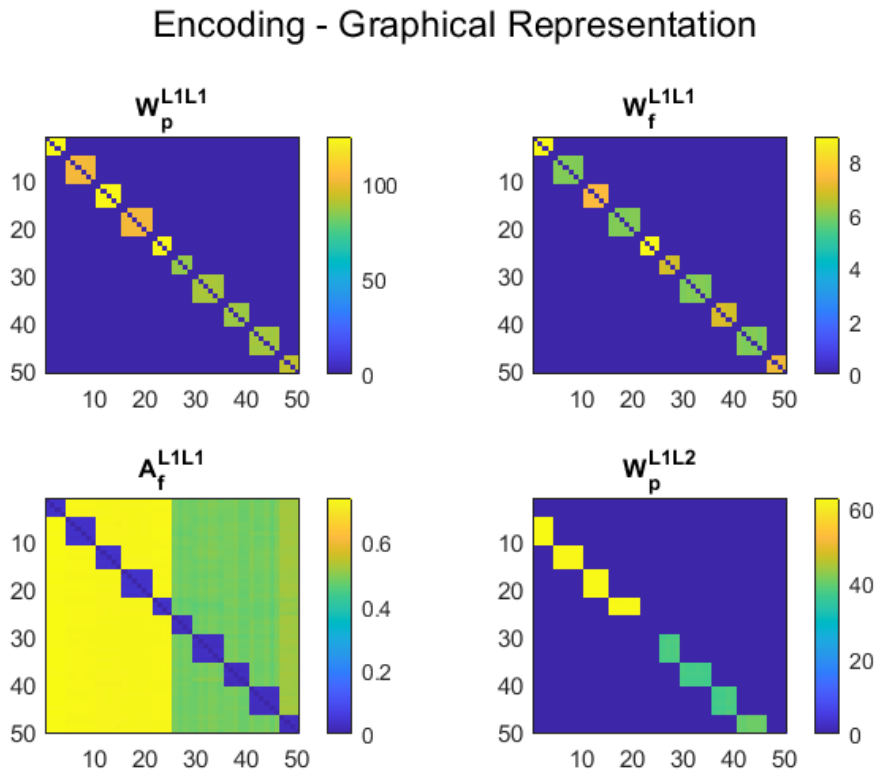

FIGURE 5.3: Colour maps of the weights values after encoding. The results are acquired by changes to k_{ach}, but the behaviour is similar for n_{ach}, too.

one. Noticeably, the weights accounting for the second sequence are weaker (thus they appear darker) than the ones on the left, graphically justifying the poor results obtained during the simulation.
As a note, the anti-Hebbian learning is distinguishable in the plot of A_f^{L1L1}, behaving in the opposite way of the other weights by activating (negatively) the features that are not currently excited; on the other hand, W_p^{L1L2} shows the temporal relation between the different episodes. In fact, each episode evokes the next in the sequence, with the exception of the last episode, ending the succession without being temporally bound with further memories.

5.1.2 Presence of Basal ACh

Unbalances in physiological functions are generally detrimental for health in both the extreme cases of underpresence or hypoactivity, and of overabundance or hyperactivity (respectively referred to the prominence of a molecule and to the operativity of any active components, such as cells or even the single proteins): this is the basis of the concept of homeostasis, for which any living entity tends to an intrinsic state of equilibrium, modulated by genetic and environmental factors [49].
The condition previously described involved a diminished binding of ACh to the

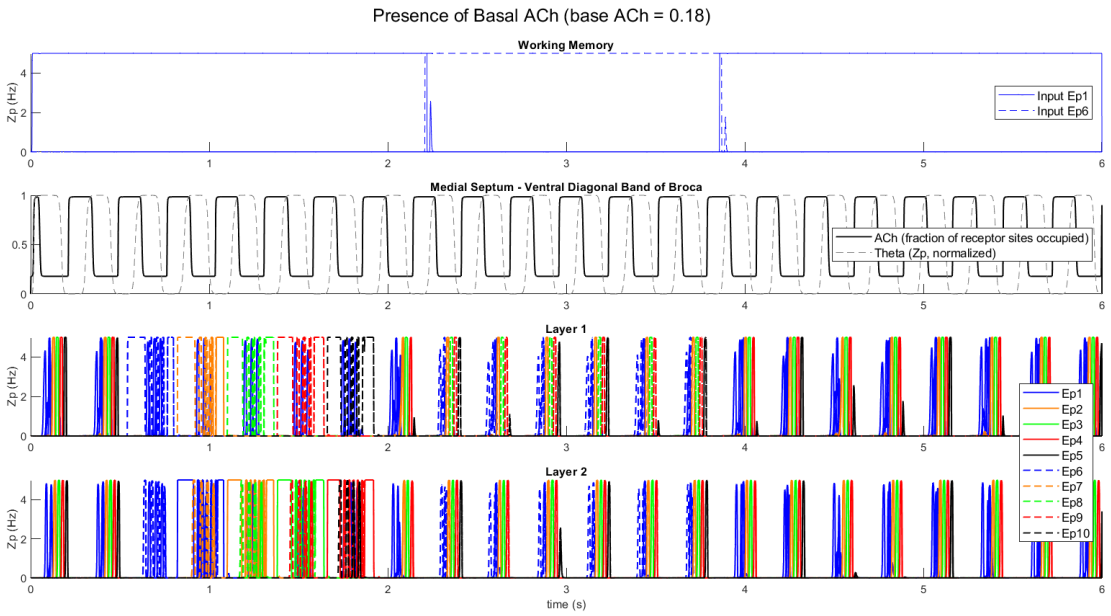

FIGURE 5.4: Results after a forced ACh binding in the range $0.18 \rightarrow 1$. Both sequences struggle to evoke all their episodes (especially the last one).

cholinergic receptors, univocally damaging the phase of encoding. In the same way, an excessive intersynaptic occupation of the neurotransmitter, due to either unrestrained release or insufficient reuptake, might introduce malfunctions in the network – this time regarding the retrieval.

The first way to evaluate such impairment would be to computationally force the ACh binding levels between a lower threshold (bigger than zero) and 1. Of course, this operation has no biological meaning, but allows for a straightforward and reliable interpretation of the results. The simulation, provided for the double-sequence case, is reported in Figure 5.4, where a sub-threshold of 18% has been chosen.

The basal presence of ACh does not affect the training of the new sequence, but instead hinders the retrieval phase of both. In fact, the first and mainly the last episode of each sequence are not properly recalled. This is due to a partial encoding (due to the non-zero ACh presence) taking place during each retrieval phase, damaging the optimally trained weights any time the sequence is recalled; the binding of the neurotransmitter also steals some of the retrieval power. Such mechanism is plainly recognizable in Figure 5.5, where a snapshot of the colour-mapped weights is provided at the time 0s, 2s and 6s.

The most affected weights are W_f^{L1L1} and A_f^{L1L1}, distinctly impaired retrieval after retrieval, with lighter weights getting darker and the opposite.

The next step in the comprehension of this condition requires finding a "natural" mechanism in our model that is able to recreate the obtained results without resorting to any force. As previously stated, an overactivation of cholinergic neurons, hence a hyper-release of the neurotransmitter in the synaptic cleft,

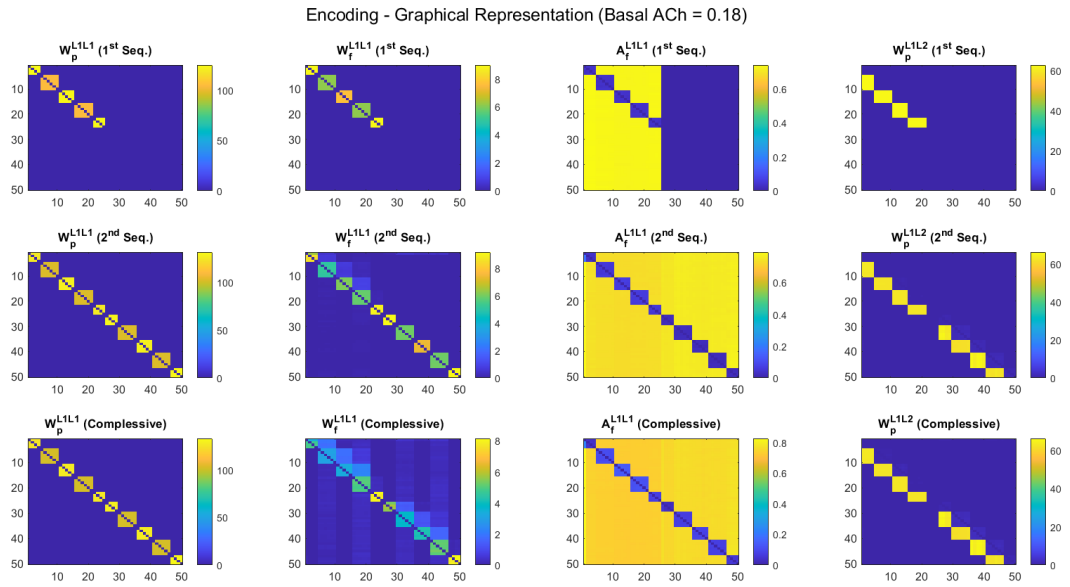

FIGURE 5.5: Training evolution at times 0s (1^{st} sequence encoded), 2s (2^{nd} sequence encoded) and 6s (complessive encoding), featuring the weights of the two sequences in colour maps.

might enable the appearance of basal ACh.
The two parameters connected to cholinergic activity are C_{fp}^{MS} and C_{cf}^{MS}; the first constant modulates the excitement of fast GABAergic interneurons, while the second ensures the inhibition of the cholinergic subpopulation. Focusing on C_{cf}^{MS} (since it directly affects cholinergic neurons) makes it evident that a weaker

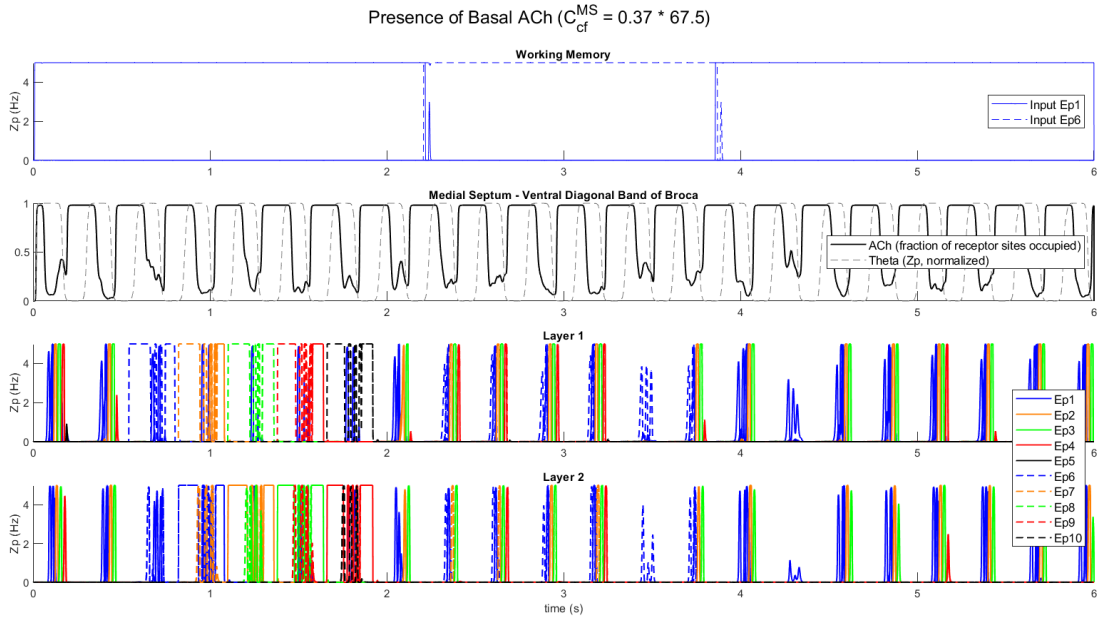

FIGURE 5.6: Simulation obtained by reducing C_{cf}^{MS} in the simultaneous encoding and retrieval case.

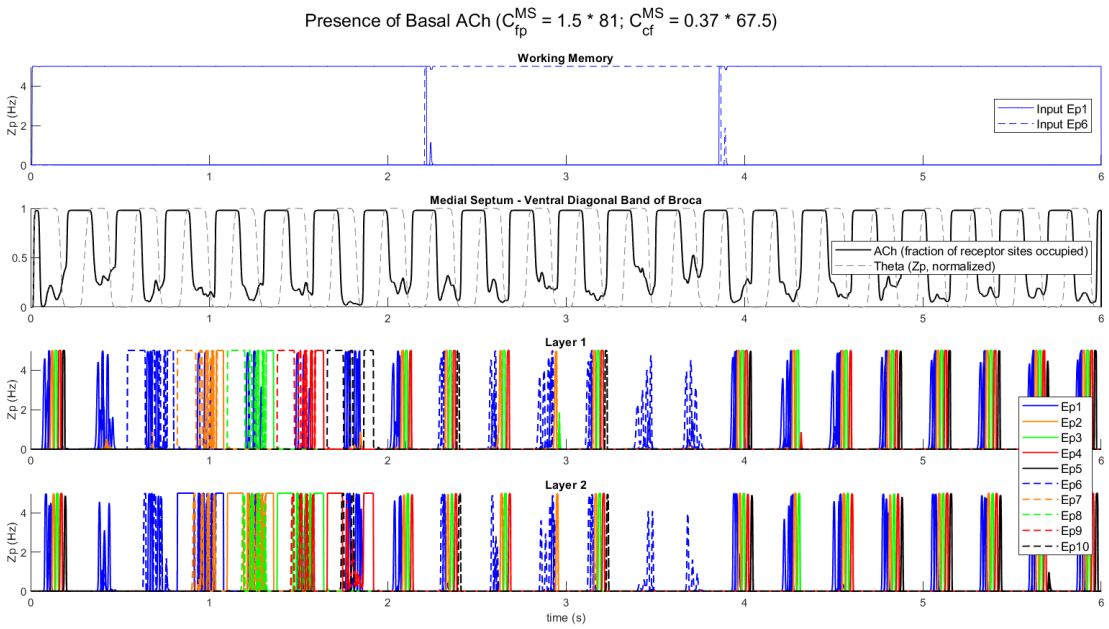

FIGURE 5.7: Results obtained from Figure 5.6 after the increase of C^{MS}_{fp}.

inhibition results in a higher presynaptic activity.
Figure 5.6 reports the outputs obtained using a very low fast-to-cholinergic connectivity. Here, the basal ACh is in average comparable to the threshold used before, but presents a much more erratic behaviour. The strength of the retrieval is related to one minus the fraction of ACh binding, therefore when the basal presence is higher, the recalling is much harder to execute, as shown in the figure.
Moreover, an increase in cholinergic duty cycle is expected from the C^{MS}_{cf} results of the sensitivity analysis: the consequence is a reduced retrieval time interval, which further damages the recalling. One way to limit this side effect is to act on C^{MS}_{fp}, increasing it so that the basal ACh binding is maintained, but the original duty cycle is as well preserved. Results of this procedure are shown in Figure 5.7. This choice undoubtedly improves the retrieval quality, allowing the sequences to reach and recall the last episode – except when the ACh residual level is too high.
It is right to add that this change could represent an actual brain mechanism to balance insufficient inhibition to cholinergic neurons, but this remains a matter of discussion and is not to be addressed here. The aim of such modifications was to analyse and comment on the presence of basal ACh and its effect on episodic memory after hypothetical (close to pathological) damages in connectivity by means of this neural mass model, which has been, in my opinion, successfully explored.

5.2 Supplementary Results

Acetylcholine is not just important for episodic memory, as we have seen, but plays a major role in the sleep-awakening cycle. A high presence of acetylcholine is related to active wakefulness, similar to REM sleep, while a lower cholinergic activity correlates with quiet wakefulness (mind wandering) and slow-wave sleep [16, 17].
All the tests and figures proposed in this thesis refer to an active state, where ACh participation is abundant (but not excessive) and the encoding-retrieval cycle is fairly balanced. By acting on the model's connectivity parameters, it is also possible to simulate low-ACh states: here the encoding process loses importance and gives way to long retrieval periods.
The recalling experienced during inactivity is not dependent on the working memory; instead, a more substantial input noise is the actual promoter of the sequences to be retrieved. The events taking place can be summarized in this way: all the features start from zero, and then the noise randomly excites them, initiating a sort of competition. At one point, the winning feature, which is the one more highly excited, will prevail on the others; this will trigger the decrease in activity of the features belonging to other episodes through the weights A_f^{L1L1}, and promote the insurgence of features belonging to its episode – and later all the following ones – through the excitatory trained weights.
Simulations of this process are shown in Figure 5.8 and Figure 5.9, respectively for slow-wave sleep and quiet waking, with additional focus on the latter in Figure 5.10. The main difference detectable is the presence of theta waves in the MS-VDB, produced during slow-wave sleep at a frequency slightly less than 3Hz. Conversely, this is not present during imagination (quiet wakefulness, characterized by non-theta state).
For completeness, the connectivity values chosen to elicit such behaviours, reported in the format *variation rate* · *default value*, were $C_{ps}^{\mathrm{MS}} = 0.65 \cdot 67.5$ and

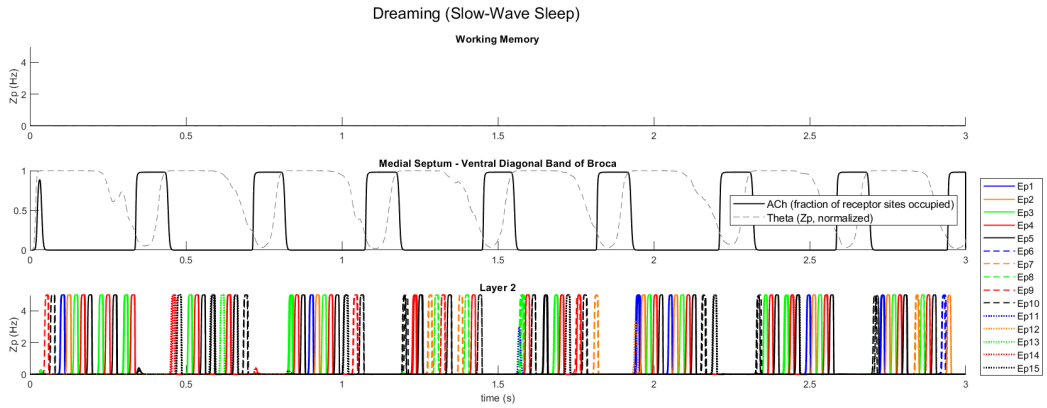

FIGURE 5.8: Slow-wave sleep emulated through low levels of cholinergic activity and high noise; only L2 is reported for clarity.

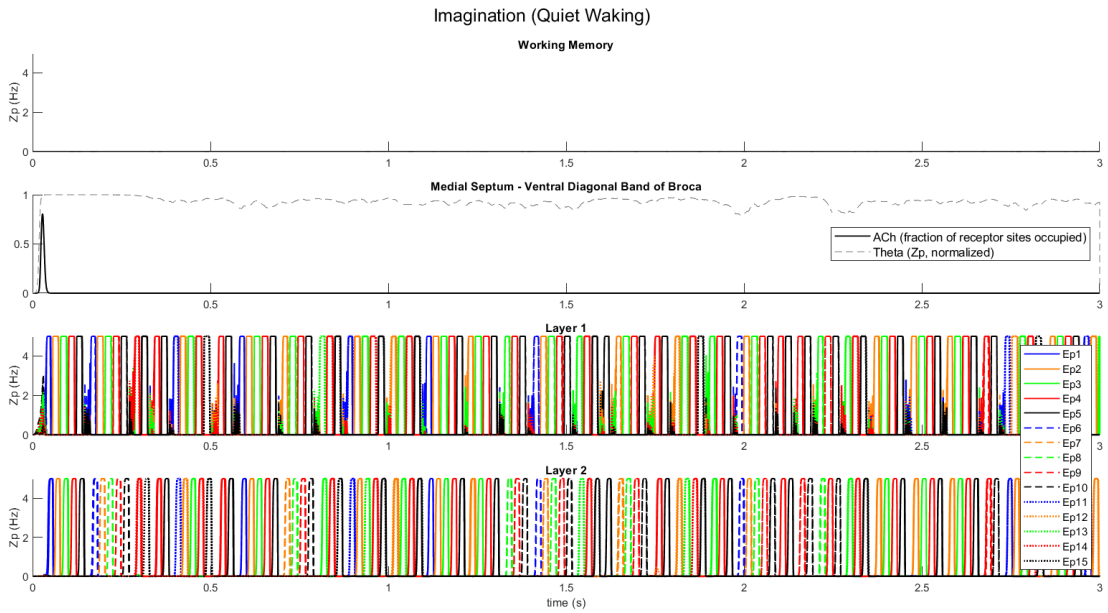

FIGURE 5.9: Simulation of the quiet waking non-theta state, much more regular in Layer 2.

$C_{fp}^{\mathrm{MS}} = 3.00 \cdot 81$ for slow-wave sleep, while the value of $C_{pe}^{\mathrm{MS}} = 1.35 \cdot 54$ was additionally used to repress theta generation in quiet waking.
Another important modification introduced in the system was the normalization of the noise based on the number of features per episode. In the original tests, in fact, the usual output episodes evoked during low-ACh states were almost exclusively the orange and the red ones, independently on the sequence. This was due to the number of features that cooperated to the recall, and it is not a surprise that the orange and red episodes possessed the highest amount. In order to obtain a more various retrieval, the noise arriving to the episodes with lower number of features was boosted by a raise in power of 1.01 (for the four-feature episodes) and 1.005 (for the five-feature ones).
This tiny change produced outputs much more homogeneous than the default

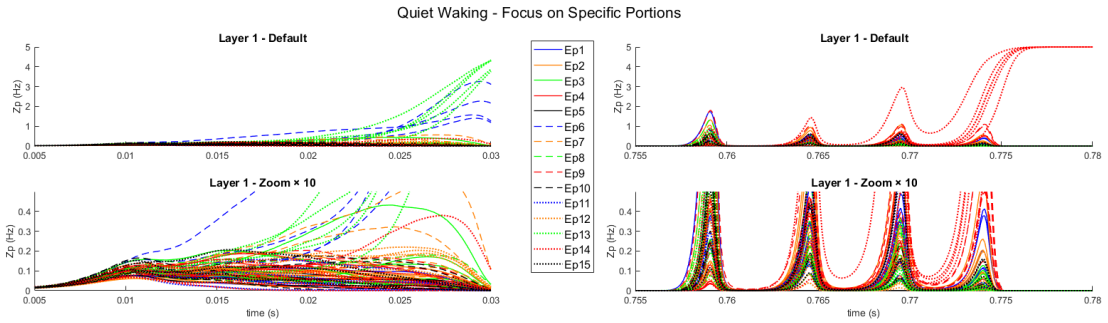

FIGURE 5.10: Layer 1 plots of the mind wandering state focusing on zoomed portions of the results. Notice how the features are randomly competing to be evoked.

scenario, flattening the recovery probability for all the fifteen different episodes. Although this choice drastically improves the consistency and, why not, the aesthetic qualities of the figures, an episode that bears more features is retrieved more often than one induced by fewer elements. This causes the imagination – or dreaming – task to revert frequently to episodes carrying more information, which is questionable.
Due to interpersonal variations and lack of broadly accepted studies, whether or not this normalization process is implemented in the brain is still debatable. New evidence [50] suggests that all the episodic data are compactly stored in single hippocampal neurons, able to later evoke spatiotemporal and sensorial memories thoroughly. This would shift the handling of episodic information to a more "democratic" approach – at least for what regards their random retrieval in absence of environmental input signals – meaning that the same neural space would be allocated for the recall of all episodes, and giving credit to the normalization procedure adopted here.

5.3 Conclusions: Strengths and Limitations

What has been discussed, implemented, and achieved up to now is a computational neural mass model for the mathematical simulation of episodic memory, built upon recent findings on the hippocampus, the MS-VDB area, and the major role of acetylcholine in the learning and recalling of sequential events.
A general explanation of the working principles of episodic memory was given at first, followed by an overall summary of the evolution of neurocomputational models preceding this one. The obtained models were then described in their functional components, and the results were provided and adequately commented. The analyses performed on ACh-linked parameters offered numerical quantities for a critical evaluation of the outputs, and paved the way for simulations in clinical settings and additional real-case scenarios.
This model was fine-tuned to memorize and recover three sequences of five episodes each, elaborating a total of 75 features each time step. Although orthogonal features are always preferable, good results were achieved even using a small percentage of features shared between two or more episodes.
The analyses of robustness and sensitivity showed that the model is relatively resistant to variations, some parameters withstanding broader changes than others. Results suggested that a proper balance in the cholinergic duty cycle, ACh binding saturation, and binding dynamics is necessary for the simultaneous accomplishment of accurate encoding and retrieval, a characteristic ability of this model.
Modifications close to pathological levels of the acetylcholine synaptic management have been tested in this chapter in the distinct cases of low ACh during encoding and in the presence of basal ACh, producing interesting insights.

Dreaming and imagination have also been successfully simulated, mimicking the actual physiological processes in a controlled and simplified environment. All these achievements were possible thanks to a complex neural mass model, improved year after year starting from the "simple" generation of multi-band signals, then grown to support the theta-gamma entrainment hypothesis, and eventually involving in this thesis the parallel handling of acetylcholine, as the fruit of the sum of more than a thousand pages of knowledge, and hours of consistent dedication.
Of course, the level reached by this model is still distant from perfection. The principal limitations encountered in its design and functionality are here concisely reported:

I. Intrinsic limits of neural mass models – as specified in Chapter 2, neural mass models are not the only option available in the construction of neuro-computational models. The advantage introduced by their implementation with respect to single neuron modeling is a reduction in the order of complexity of the system, resulting in faster and still accurate emulations. Despite this, ideal models should aim to very high levels of accuracy and biological realism, potentially taking into account multiple neuronal types and spatial disposition, including synaptic plastic distribution. Even though being impossible these days, such implementation might just be a few papers down the line.

II. Computational areas – the regions included in this model are WM (medial-prefrontal cortex), MS-VDB, L1 (CA3) and L2 (CA1). This organization is functional and effective, but more areas could be involved for a more precise simulation of episodic memory, such as the EC, the dentate gyrus and so on.

III. Features and episodes – several simplifications have been adopted regarding the essence of episodic features in the simulations: each episode contained from four to six orthogonal (or a few shared) features, and each temporal sequence was strictly composed of five episodes. The features in this work had no biological relevance; no sensorial nor spatial meaning was actually implied in their functioning. Furthermore, the number of features held by each episode is arbitrary, and no test has been performed on sequences of shorter or longer length. Despite this, it is safe to add that such a level of realism was not intended to be achieved in this model, which aim was to generally assess ACh-mediated encoding and recovery of hypothetical mnemonic elements. Certainly, the acquisition of a stronger physiological significance will be a matter of the next works.

IV. Sensory evidence and encoding – sensorial information is supposed to be received constantly from the EC during each encoding phase, but this

operative choice could be criticised as being too simplistic: in fact, data processing in the entorhinal-hippocampal system follows the theta-gamma coupling, meaning that sensorial signals are not constantly obtained, but are received at a gamma fast (60-90Hz) frequency band [51]. Modifications of the encoding process will be therefore needed in future studies to include such evidence.

These aspects, together with the overall discussion carried out during the model analyses and the commented results, highlight the present state of neurocomputational evaluation of episodic memory and indicate a few ways to improve the quality of upcoming simulations.
Nevertheless, it is impossible to predict exactly what the next discoveries will be like, seen how fast research is flourishing in the fields of neuroscience, neurocomputational modeling, biomedical imaging, as well as in closely-related promising domains such as neurorobotics, artificial intelligence, quantum computing, and the list goes on and on.
It is always spectacular to actively witness as multiple scientific fields encounter, enriching mankind's knowledge with the wholehearted intention of granting long, peaceful, thrilling and inspiring lives to everyone.
It is even more impressive to realise how all of this is made true, out of mere words and some colourful pixels.
Just like these pages.

List of Figures

List of Tables

Bibliography

[1] Timothy A. Allen and Norbert J. Fortin. 'The evolution of episodic memory'. In: *PNAS* 110.supplement 2 (2013). DOI: 10.1073/pnas.1301199110.

[2] Jørgen Sugar and May-Britt Moser. 'Episodic memory: Neuronal codes for what, where, and when'. In: *Hippocampus* 29.12 (2019), pp. 1190–1205. DOI: 10.1002/hipo.23132.

[3] Francesca Tozzi. 'Specific contribution of the Lateral Entorhinal Cortex to episodic-like memory recall'. In: (2024). URL: https://dx.doi.org/10.25429/tozzi-francesca_phd2024-02-28.

[4] Krubeal Danieli, Alice Guyon and Ingrid Bethus. 'Episodic Memory formation: A review of complex Hippocampus input pathways'. In: *Progress in Neuro-Psychopharmacology and Biological Psychiatry* 126 (2023), p. 110757. DOI: 10.1016/j.pnpbp.2023.110757.

[5] George A. Miller. 'The magical number seven, plus or minus two: Some limits on our capacity for processing information'. In: *THE PSYCHOLOGICAL REVIEW* 63.2 (1955), pp. 81–97. DOI: 10.1037/h0043158.

[6] Nelson Cowan. 'The magical number 4 in short-term memory: A reconsideration of mental storage capacity'. In: *Behavioral and Brain Sciences* 24.1 (2001), pp. 87–114. DOI: 10.1017/S0140525X01003922.

[7] Clarence Green. 'Usage-based linguistics and the magic number four'. In: *Cognitive Linguistics* (2017). DOI: 10.1515/cog-2015-0112.

[8] Mingtao Lu. 'Magic Number 7: A Behavioral Economic Analysis of Miller's Rule'. In: *Chongqing Technology and Business University, Social Science Edition* (2011). URL: https://ssrn.com/abstract=1771142.

[9] John E. Lisman and Ole Jensen. 'The Theta-Gamma Neural Code'. In: *Neuron* 77.6 (2013), pp. 1002–16. DOI: 10.1016/j.neuron.2013.03.007.

[10] Michael E. Hasselmo. 'Septal Modulation of Hippocampal Dynamics: What Is the Function of the Theta Rhythm?' In: *The Behavioral Neuroscience of the Septal Region* (2000). DOI: 10.1007/978-1-4612-1302-4_5.

[11] Bálint Király et al. 'The medial septum controls hippocampal supra-theta oscillations'. In: *Nature Communications* 14 (2023), p. 6159. DOI: 10.1038/s41467-023-41746-0.

[12] György Buzsáki and Xiao-Jing Wang. 'Mechanisms of Gamma Oscillations'. In: *Annu Rev Neurosci.* 35 (2012), pp. 203–225. DOI: 10.1146/annurev-neuro-062111-150444.

[13] D. Yves von Cramon and Uwe Schuri. 'The Septo-Hippocampal Pathways and Their Relevance to Human Memory: A Case Report'. In: *Cortex* 28.3 (1992), pp. 411–422. DOI: 10.1016/S0010-9452(13)80151-7.

[14] Vincent Douchamps et al. 'Evidence for Encoding versus Retrieval Scheduling in the Hippocampus by Theta Phase and Acetylcholine'. In: *Journal of Neuroscience* 33.20 (2013), pp. 8689–8704. DOI: 10.1523/JNEUROSCI.4483-12.2013.

[15] Christian Sam and Bruno Bordoni. 'Physiology, Acetylcholine'. In: *StatPearls [Internet]* (2023). URL: https://www.ncbi.nlm.nih.gov/books/NBK557825.

[16] Ann E. Power. 'Slow-wave sleep, acetylcholine, and memory consolidation'. In: *PNAS* 101.7 (2004), pp. 1795–1796. DOI: 10.1073/pnas.0400237101.

[17] Michael E Hasselmo. 'The role of acetylcholine in learning and memory'. In: *Current Opinion in Neurobiology* 16.6 (2006), pp. 710–715. DOI: 10.1016/j.conb.2006.09.002.

[18] Krubeal Danieli, Alice Guyon and Ingrid Bethus. 'Episodic Memory formation: A review of complex Hippocampus input pathways'. In: *Progress in Neuro-Psychopharmacology and Biological Psychiatry* 126 (2023), p. 110757. DOI: 10.1016/j.pnpbp.2023.110757.

[19] Michael B. Bone and Bradley R. Buchsbaum. 'Detailed Episodic Memory Depends on Concurrent Reactivation of Basic Visual Features within the Posterior Hippocampus and Early Visual Cortex'. In: *Cerebral Cortex Communications* 2 (2021), pp. 1–15. DOI: 10.1093/texcom/tgab045.

[20] Michael E. Hasselmo and James L. McClelland. 'Neural models of memory'. In: *Cerebral Cortex Communications* 9.2 (1999), pp. 184–188. DOI: 10.1016/S0959-4388(99)80025-7.

[21] 'Learning from the brain to make AI more energy-efficient'. In: *Human Brain Project* (2023). URL: https://www.humanbrainproject.eu/en/follow-hbp/news/2023/09/04/learning-brain-make-ai-more-energy-efficient.

[22] Mark Nelson and John Rinzel. 'The Hodgkin-Huxley Model'. In: *The book of genesis* (1995). URL: http://genesis-sim.org/GENESIS/Ultimate_CDROM/Tutorials/iBoGpdf/chapt4.pdf.

[23] J. Nagumo amd S. Arimoto and S. Yoshizawa. 'An Active Pulse Transmission Line Simulating Nerve Axon'. In: *Proceedings of the Ire* (1962), pp. 2061–2070. DOI: 10.1109/JRPROC.1962.288235.

[24] Eugene M. Izhikevich. 'Which Model to Use for Cortical Spiking Neurons?' In: *IEEE TRANSACTIONS ON NEURAL NETWORKS* 15.5 (2004), pp. 1063–1070. DOI: 10.1016/S0959-4388(99)80025-7.

[25] A. N. Burkitt. 'A Review of the Integrate-and-fire Neuron Model: I. Homogeneous Synaptic Input'. In: *Biological Cybernetics* 95 (2006), pp. 1–19. DOI: 10.1007/s00422-006-0068-6.

[26] Eugene M. Izhikevich. 'Dynamical systems in neuroscience'. In: *MIT Press* (2007). ISBN: 978-0262514200.

[27] Kashu Yamazaki et al. 'Spiking Neural Networks and Their Applications: A Review'. In: *Brain Sciences* 12.7 (2022), p. 863. DOI: 10.3390/brainsci12070863.

[28] Hugh R. Wilson and Jack D. Cowan. 'Excitatory and Inhibitory Interactions in Localized Populations of Model Neurons'. In: *Biophysical Journal* 12.1 (1972), pp. 1–24. DOI: 10.1016/S0006-3495(72)86068-5.

[29] Ben H. Jansen, George Zouridakis and Michael E. Brandt. 'A neurophysiologically-based mathematical model of flash visual evoked potentials'. In: *Biological Cybernetics* 68 (1993), pp. 275–283. DOI: 10.1007/BF00224863.

[30] Ben H. Jansen and Vincent G. Rit. 'Electroencephalogram and visual evoked potential generation in a mathematical model of coupled cortical columns'. In: *Biological Cybernetics* 73 (1995), pp. 357–366. DOI: 10.1007/BF00199471.

[31] Lopes da Silva et al. 'Model of brain rhythmic activity - The alpha-rhythm of the thalamus'. In: *Kibernetic* 15.1 (1974), pp. 27–37. DOI: 10.1007/BF00270757.

[32] F. Wendling et al. 'Epileptic fast activity can be explained by a model of impaired GABAergic dendritic inhibition'. In: *European Journal of Neuroscience* 15.9 (2002), pp. 1499–1508. DOI: 10.1046/j.1460-9568.2002.01985.x.

[33] Mauro Ursino, Filippo Cona and Melissa Zavaglia. 'The generation of rhythms within a cortical region: Analysis of a neural mass model'. In: *NeuroImage* 52.3 (2010), pp. 1080–1094. DOI: 10.1016/j.neuroimage.2009.12.084.

[34] Roberto Sotero et al. 'Realistically coupled neural mass models can generate EEG rhythms'. In: *NeuroImage* 19.2 (2007), pp. 478–512. DOI: 10.1162/neco.2007.19.2.478.

[35] Melissa Zavaglia et al. 'A neural mass model for the simulation of cortical activity estimated from high resolution EEG during cognitive or motor tasks'. In: *Journal of Neuroscience Methods* 157.2 (2006), pp. 317–329. DOI: 10.1016/j.jneumeth.2006.04.022.

[36] R.J. Moran et al. 'A neural mass model of spectral responses in electrophysiology'. In: *NeuroImage* 37.3 (2007), pp. 706–720. DOI: 10.1016/j.neuroimage.2007.05.032.

[37] R.J. Moran et al. 'Dynamic causal models of steady-state responses'. In: *NeuroImage* 44.3 (2009), pp. 796–811. DOI: 10.1016/j.neuroimage.2008.09.048.

[38] Filippo Cona et al. 'Changes in EEG Power Spectral Density and Cortical Connectivity in Healthy and Tetraplegic Patients during a Motor Imagery Task'. In: *Computational Intelligence and Neuroscience* (2009). DOI: 10.1155/2009/279515.

[39] Gabriele Pirazzini and Mauro Ursino. 'Modeling the contribution of theta-gamma coupling to sequential memory, imagination, and dreaming'. In: *Frontiers in Neural Circuits* 18 (2024). DOI: 10.3389/fncir.2024.1326609.

[40] Utkarsh Utkarsh et al. 'Automated translation and accelerated solving of differential equations on multiple GPU platforms'. In: *Computer Methods in Applied Mechanics and Engineering* 419 (2024). DOI: 10.1016/j.cma.2023.116591.

[41] Spyridon Chavlis et al. 'Dendrites of dentate gyrus granule cells contribute to pattern separation by controlling sparsity'. In: *Hippocampus* 27.1 (2016), pp. 89–110. DOI: 10.1002/hipo.22675.

[42] Jennifer C. Robinson et al. 'Septo-hippocampal dynamics and the encoding of space and time'. In: *Trends in Neurosciences* 46.9 (2023), pp. 712–725. DOI: 10.1016/j.tins.2023.06.004.

[43] Sylvain Goutelle et al. 'The Hill equation: a review of its capabilities in pharmacological modelling'. In: *Fundamental and Clinical Pharmacology* 22.6 (2008), pp. 633–648. DOI: 10.1111/j.1472-8206.2008.00633.x.

[44] Paul J. Whiting and Jon M. Lindstrom. 'Purification and characterization of a nicotinic acetylcholine receptor from chick brain'. In: *Biochemistry* 25.8 (1986), pp. 2082–2093. DOI: 10.1021/bi00356a037.

[45] Michael Graupner and ohers. 'Endogenous Cholinergic Inputs and Local Circuit Mechanisms Govern the Phasic Mesolimbic Dopamine Response to Nicotine'. In: *PLOS Computational Biology* (2013). DOI: 10.1371/journal.pcbi.1003183.

[46] Casper Kerrén. 'An Optimal Oscillatory Phase for Pattern Reactivation during Memory Retrieval'. In: *Current Biology* 28 (2018), pp. 3383–3392. DOI: 10.1016/j.cub.2018.08.065.

[47] William J. Brammar. 'Entry 09 - ELG CAT nAChR: Nicotinic acetylcholine-gated integral receptor–channels'. In: *Ion Channel Factsbook* (1996), pp. 234–292. DOI: 10.1016/B978-012184450-9/50009-0.

[48] Michael Graupner et al. 'Endogenous cholinergic inputs and local circuit mechanisms govern the phasic mesolimbic dopamine response to nicotine'. In: *PLoS Comput Biol.* 9.8 (2013). DOI: 10.1371/journal.pcbi.1003183.

[49] Kelvin J.A. Davies. 'Adaptive homeostasis'. In: *Molecular Aspects of Medicine* 49 (2016), pp. 1–7. DOI: 10.1016/j.mam.2016.04.007.

[50] Luca D. Kolibius et al. 'Hippocampal neurons code individual episodic memories in humans'. In: *Nature Human Behaviour* 7 (2023), pp. 1968–1979. DOI: 10.1038/s41562-023-01706-6.

[51] Laura Lee Colgin. 'Theta–gamma coupling in the entorhinal–hippocampal system'. In: *Current Opinion in Neurobiology* 31 (2015), pp. 45–40. DOI: 10.1016/j.conb.2014.08.001.

Acknowledgements

As the years at *uni* passed by, five `l o n g` years of laughs, tears, panic, enthusiasm, bus rides and maze-like corridors, I want to thank from the bottom of my heart all the people that even just shared a look with me, since they metamorphosed me into what I am today: an emotive nerd with unexplainable passion for cute robots and neurons.

First of all, I want to thank Gabriele and "the prof" Ursino, the two big brains that made this thesis possible, supporting me with their kindness, expertise, and bursts of excitement.

Then I must thank my unforgettable companions, Ale, Bubu, Cami, Dave, Jai, Lori, Ludo, Mani, Sere, and mythical Vitto, a collection of wonderful souls and splendid friends.

Thanks to the IMPERO, mad people with crazy personalities spreading the deepest of the love to anyone they meet.

I must thank mamma, babbo and the bros, mainly for their patience and secondly for their strength and natural goodness.

And as last my pookie Peter, because even after almost four years, I haven't stop discovering how special you are, and yes, we'll manage to get that greenhouse done somewhere in the garden, maybe near the willow.
But it'll be hexagonal, that's for sure.

Nicolas